IVYSPRING INTERNATIONAL PUBLISHER

Theranostics

2018; 8(22): 6322-6349. doi: 10.7150/thno.27828

Review

Dendrimer- and copolymer-based nanoparticles for magnetic resonance cancer theranostics

Sayoni Ray[1*], Zhao Li[1*], Chao-Hsiung Hsu[1,2*], Lian-Pin Hwang[2], Ying-Chih Lin[2], Pi-Tai Chou[2], Yung-Ya Lin[1]✉

1. Department of Chemistry and Biochemistry, University of California, Los Angeles, CA 90095, USA
2. Department of Chemistry, National Taiwan University, Taipei 10617, Taiwan

* These authors contributed equally to this work.

✉ Corresponding author: Yung-Ya Lin, Email- yylin@chem.ucla.edu, Tel- (310) 206-2856

Received: 2018.06.12; Accepted: 2018.09.20; Published: 2018.11.29

Abstract

Cancer theranostics is one of the most important approaches for detecting and treating patients at an early stage. To develop such a technique, accurate detection, specific targeting, and controlled delivery are the key components. Various kinds of nanoparticles have been proposed and demonstrated as potential nanovehicles for cancer theranostics. Among them, polymer-like dendrimers and copolymer-based core-shell nanoparticles could potentially be the best possible choices. At present, magnetic resonance imaging (MRI) is widely used for clinical purposes and is generally considered the most convenient and noninvasive imaging modality. Superparamagnetic iron oxide (SPIO) and gadolinium (Gd)-based dendrimers are the major nanostructures that are currently being investigated as nanovehicles for cancer theranostics using MRI. These structures are capable of specific targeting of tumors as well as controlled drug or gene delivery to tumor sites using pH, temperature, or alternating magnetic field (AMF)-controlled mechanisms. Recently, Gd-based pseudo-porous polymer-dendrimer supramolecular nanoparticles have shown 4-fold higher T_1 relaxivity along with highly efficient AMF-guided drug release properties. Core-shell copolymer-based nanovehicles are an equally attractive alternative for designing contrast agents and for delivering anti-cancer drugs. Various copolymer materials could be used as core and shell components to provide biostability, modifiable surface properties, and even adjustable imaging contrast enhancement. Recent advances and challenges in MRI cancer theranostics using dendrimer- and copolymer-based nanovehicles have been summarized in this review article, along with new unpublished research results from our laboratories.

Key words: dendrimer nanoparticle, copolymer nanoparticle, magnetic resonance, cancer theranostics

1. Magnetic resonance cancer theranostics

Theranostics refers to the development of molecular diagnostics and targeted therapeutics in an interdependent, collaborative manner. Nano-theranostics takes advantage of the high capacity of nano-platforms to ferry cargo and load onto them both imaging and therapeutic functions. The resulting nanosystems, which are capable of diagnosis, drug delivery, and monitoring of therapeutic response, are expected to play a significant role in the dawning era of personalized medicine, and much research effort has been devoted toward that goal. For example, magnetic resonance (MR) nano-theranostics uses magnetic nanoparticles for cancer detection by MR molecular imaging and for cancer therapy by MR nanomedicine. Through active and passive targeting mechanisms, the magnetic nanoparticles can serve as "molecular beacons" to enhance the MR image contrast for early lesion detection. Moreover, through interacting with external alternating magnetic fields produced by the MR hardware, these magnetic

nanoparticles accumulated at the lesions can generate heat to serve as "molecular bullets" to kill cancer cells directly through hyperthermia or indirectly through thermal activation and controlled release of drugs.

Cancer theranostic approaches include three major components: (i) detection, (ii) targeting, (iii) controlled delivery and release [1–7]. For detection, several methods including positron emission tomography (PET), computed tomography (CT), single-photon emission computed tomography (SPECT), fluorescence, near-infrared (NIR) radiation spectroscopy, and magnetic resonance imaging (MRI) have been used [4]. Among these techniques, MRI serves as a powerful, noninvasive tool for cancer detection and is commonly used worldwide. However, MRI suffers a major drawback—limited contrast between the healthy and malignant tissues in the early stages of cancers. Hence, much effort has been invested to enhance the tumor contrast in MRI by using different types of contrast agents. At present, gadolinium (Gd) and superparamagnetic iron oxide (SPIO) are the most widely used contrast agents in the clinical setups [8–12].

While a considerable amount of work has been invested in improving Gd and SPIO-based MRI contrast agents, accurate targeting of cancer cells remains a fundamental challenge for cancer theranostics. Conventional chemotherapy cannot distinguish between the healthy cells and diseased cells, and consequently results in the death of a large number of healthy cells. To alleviate this problem, a safer approach of targeted drug delivery is highly desirable. Effective targeting using nanovehicles would allow for a lower administered dosage of therapeutics, thus minimizing the adverse side effects that are major problems for either active or passive targeting.

A common challenge for all types of cancer therapies is the unwanted damage to healthy cells while treating the malignant tumor. Hence, a primary goal of any type of cancer therapy (chemotherapy, gene therapy, immunotherapy, induced hyperthermia, radiotherapy, *etc.*) is to deliver the required drug or gene to the malignant tumor site only and to reduce the damage to healthy cells. For this purpose, a suitable biocompatible and preferably biodegradable nanovehicle is required to deliver the therapeutics to the tumor site, while minimizing any unwanted side effects. The drug release from the nanovehicle is commonly controlled by heat, temperature, or pH values. For example, magnetic hyperthermia could be induced and exploited by coupling the magnetic dipoles of SPIO nanoparticles to an external alternating magnetic field [13], producing heat to kill the drug-resistant cancer cells. Alternatively, the heat generated could be used to manipulate thermosensitive drug carriers for controlled drug release or to activate extracellular heat shock proteins for antitumor immune responses [14]. Particularly, a nanovehicle carrying the drug via an acid cleavable bond could be used for drug delivery by releasing the drug upon approaching the more acidic tumor microenvironment [15]. An effective drug targeting and delivery method would require a suitable and biocompatible nanovehicle to carry the drug and to serve as a contrast-enhancing agent that could be conjugated to different targeting moieties for efficient detection.

In this review, we summarize various approaches to cancer theranostics within the scope of magnetic resonance with simultaneous diagnosis and treatment. At present, a worldwide effort is going on in search of suitable nanovehicles for this purpose [16]. In this context, polymer-based nanoparticles are considered more attractive and feasible because of their controllable size and biocompatibility [17]. The scope of this review article is to discuss the current status of research regarding the use of polymer-like dendrimer (**Figure 1**) and core-shell copolymer-based (**Figure 2**) nanoparticles as nanovehicles for use in cancer therapy in conjunction with MRI-guided detection, diagnosis and treatment. The development of novel nano-biomaterials for contrast agents, targeting, and drug delivery is beyond the scope of this review and can be found in these references [1–4, 8, 14]. We aim to summarize the most recent advances and directions of dendrimer and core-shell copolymer-based, MRI-guided, theranostic approaches to cancer treatment, including published and unpublished work from our laboratories.

2. Dendrimer-based nanoparticles for MR cancer theranostics

The dendrimer molecule has polymer-like repetitive structures with a symmetric, almost spherical shape. Most of the polymers are not water-soluble. However, the dendrimers can be made water-soluble if needed. A schematic diagram of the dendrimer is shown in **Figure 1**. The dendrimer is used as a versatile drug delivery nanovehicle in nanomedicine. Its flexible structure allows for a wide variety of molecules to be conjugated to the exterior while it is still capable of carrying different kinds of drugs by forming covalent or non-covalent bonds within the core [18]. Dendrimers can modify hydrophobic quantum dots to water-soluble hydrophilic dots and such properties have recently attracted a lot of attention due to the presence of more functional groups at a higher density compared to other linear ligands. For example, the presence of

dense ligand layer and the strong inter-ligand interaction in polyamidoamine (PAMAM) dendrimer makes it thermally, chemically and photochemically more stable in comparison to the other hydrophilic ligands with thinner layer. The presence of various anchoring groups increases its versatility for interacting with different ligands for targeting, drug loading and encapsulating contrast agents. Furthermore, the terminal groups can be modified to attach to other biomolecules and reduce their toxicity to benign tissues. These special features make them excellent coating agents as well as nanovehicles [19].

Nanoparticle biodistribution and targeting depend on the size, shape, and heterogeneity of the nanoparticles. The controllable size of the dendrimer is one of its important advantages for cancer therapy applications. Although the dendrimer is highly branched, it has a symmetrical structure as well as a low polydispersity index, reflecting the homogeneous size distribution of the particles. These properties allow the dendrimer to be used for targeting and treating cancer cells [20–22]. Larger particles could be easily identified as foreign objects and eliminated from the body by the mononuclear phagocyte system (MPS), whereas particles smaller than 5–6 nm could be removed via renal filtration [8]. To increase the circulation time within the body for adequate drug delivery, the optimal size of the nanoparticles should be in the range of 10 nm to 100 nm approximately. The size of the dendritic nanovehicle can be optimized to prolong the circulation time within the body. Moreover, the unique topology of the dendrimer helps it circulate in the bloodstream much longer than a linear polymer.

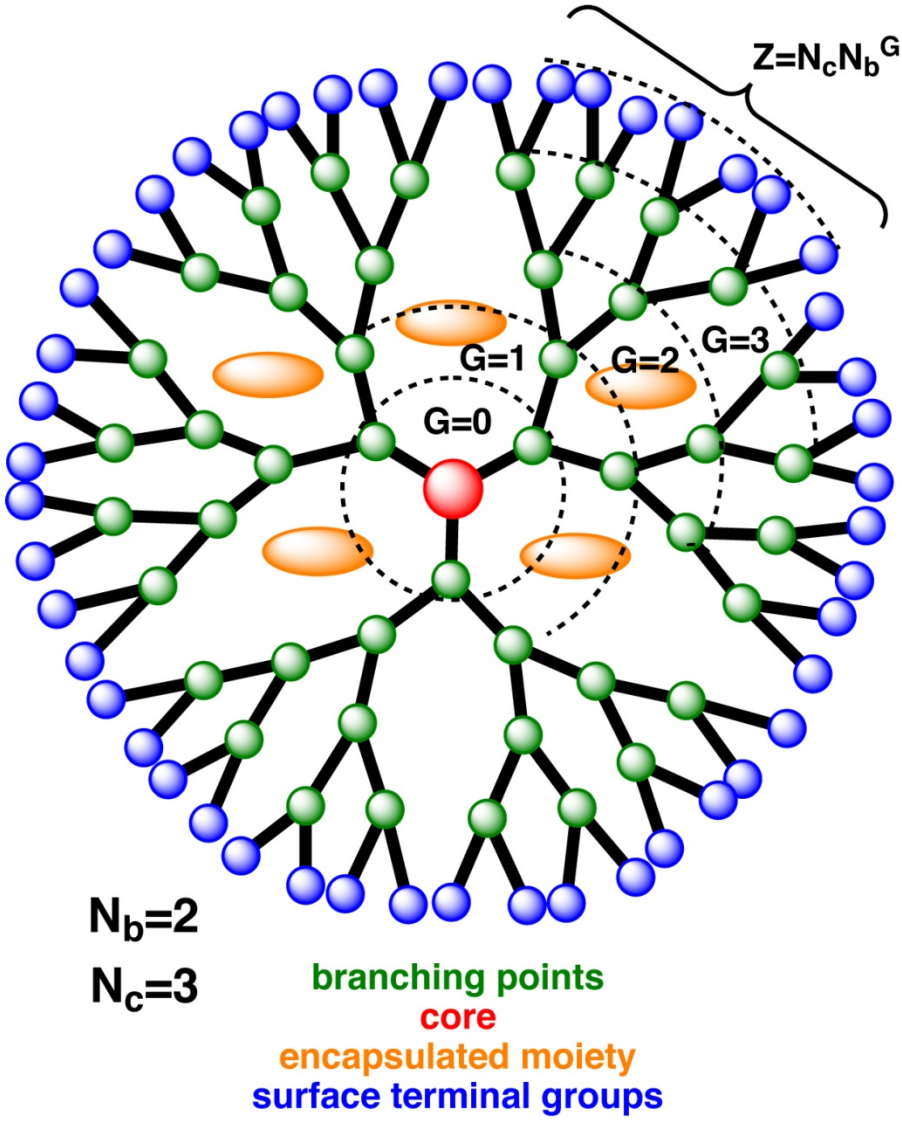

Figure 1. Schematic diagram of dendrimer, illustrating core (red), branching points (green), surface terminal groups (blue), and position of encapsulated moiety (orange) that can be contrast agent or drug. The dotted spherical boundaries dictate the generation (G). G = 0 for the core, G = 1 for the next concentric shell, and so on. N_c represents the number of branches in the core, whereas N_b is the branch cell multiplicity. In this figure, N_c = 3 and N_b = 2, which gives the total number of surface terminal groups, $Z = N_c N_b^G$ = 48.

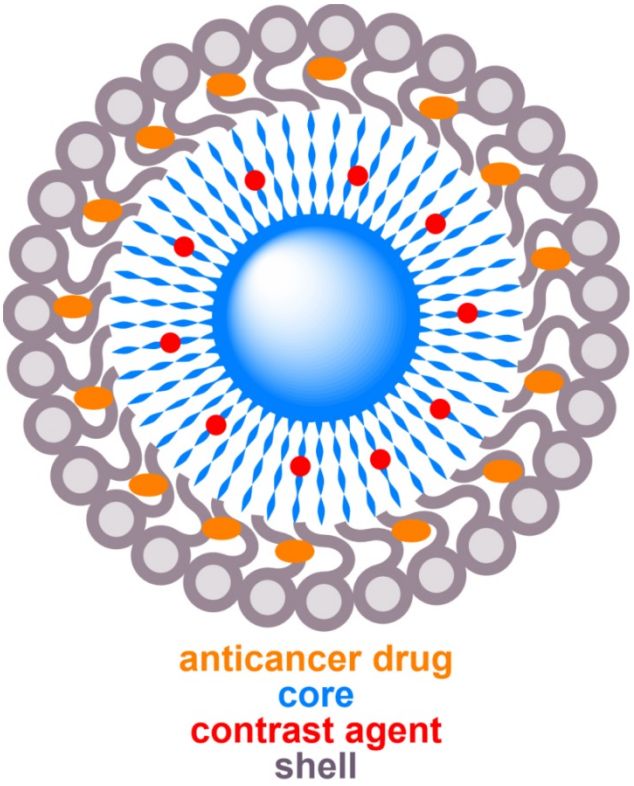

Figure 2. Schematic diagram of a typical core-shell structure formed by copolymers, illustrating core (blue), shell (grey), MRI contrast agent (red), and anticancer drug (orange).

The dendrimer composition may include a wide variety of substances depending on its applications [18, 21, 23]. For example, the PAMAM dendrimer is one of the most commonly used classes of dendrimers due to its highly symmetric, multi-branched, spherically ordered structure, and biocompatibility [23, 24]. While a large variety of dendrimer compositions have become available in recent years, different generations (G) of dendrimers have also been explored simultaneously in different studies. Generation is a parameter used to classify dendrimers into categories based on their size and branching properties, as depicted in **Figure 1**. The terminal surface group (Z) of the dendrimer is related to the core multiplicity (N_c) and branch cell multiplicity (N_b) with generation (G), such that $Z = N_c N_b^G$ [20]. Different generations of dendrimers have distinct spacing and branching features. Void space between the branches and the concentration of exterior branches determines the dendrimer's capability of entrapping and releasing drug molecules, and optimal ratios for conjugation of targeting moieties. Additionally, the dendrimers show generation-dependent cytotoxicity, pharmacokinetics, and biodistribution behaviors [25]. Therefore, a proper choice of generation is crucial in order for the dendrimer to serve as an efficient delivery nanovehicle. Recent therapeutic applications revolve around the use of generation 2.5–5 dendritic nanovehicles [26], as they possess lower cytotoxicity from non-specific drug release at healthy tissue sites in comparison to other conventionally used cationic polymers.

In the following, we will summarize various approaches to functionalize dendrimers for targeting, detection, and drug delivery with minimal side effects under the guidance of MRI techniques. In **Table 1**, we present a short overview of different possible dendrimer-related therapeutic advances of this field in recent years, with the key details of imaging, targeting approaches, drugs, delivery mechanisms, and types of cancers.

2.1. T_2-mode SPIO-based dendrimer nanoparticles

Dendrimer-coated SPIO nanoparticles are one type of ideal candidate for theranostic applications. These complexes are particularly useful for their adjustable size, biocompatibility and low toxicity [27, 28]. In recent years, SPIOs have been studied extensively as an important T_2 contrast agent that could exhibit high transverse relaxivity in MRI. This higher relaxivity produces a negative contrast in MRI T_2-weighted imaging. The exact position of the tumor can be determined by this negative contrast, as the MR signal decreases at the malignant tumor site at a faster rate in comparison to that at healthy tissue.

Magnetic nanoparticles can serve as "molecular beacons" to enhance the MR image contrast for early lesion detection through active (e.g., antibody–antigen) and passive (e.g., enhanced permeability and retention effect, EPR) targeting mechanisms. An effective form of active targeting involves exploitation of the magnetic properties of the nanoparticles under a magnetic field gradient known as magnetofection [29, 30]. If an external magnet is placed near the tumor, the magnetic nanoparticles experience a driving force under the inhomogeneous magnetic field, resulting in accumulation of particles at the tumor site. This active targeting is superior to passive targeting where the latter relies on EPR. In passive targeting, nanoparticles and macromolecular drugs of specific sizes tend to accumulate in tumor tissue much more than they do in normal tissues [31, 32], which is known as the EPR effect. Such phenomenon could be explained by the stimulated production of blood vessels from proximal fast-growing malignant tumor cells. These newly formed vessels at the tumor site are usually abnormal in form and architecture, which leads to abnormal molecular and fluid transport dynamics. The EPR effect helps deliver and distribute the nanoparticles inside the cancer tissue, resulting in

passive targeting. However, surface-functionalized SPIO showed better EPR effects in blood, enhanced stability, and had less potential of becoming agglomerated [27].

Table 1. Theranostic approaches using functionalized dendrimer.

Imaging probe	Dendrimer	Drug	Targeting approach	Delivery mechanism	Cancer	Ref.
SPIO (T_2 MRI)	G4 PAMAM modified with poly I:C	DOX	N/A [a]	pH-responsive	*In vitro*: breast cancer (MCF-7)	34
SPIO (T_2 MRI)	G4 PAMAM	DOX	N/A [a]	pH-responsive	*In vitro*: breast cancer (MCF-7)	35
SPIO (T_2 MRI)	G0 PAMAM	Gemcitabine	ATRA [a]	pH-responsive	*In* vitro: pancreatic cancer (SU86.86, T3M4, PANC-1)	38
SPIO (T_2 MRI)	G3.5 PAMAM	DOX	FA [a]	pH-responsive (hydrazone bond)	*In vivo*: melanoma (B16-F0 s.c.)	43
SPIO (T_2 MRI)	G2.5 PAMAM	DOX	FA [a]	pH-responsive (hydrazone bond)	*In vivo*: melanoma (B16-F0 s.c.)	44
SPIO (T_2 MRI)	G4 PAMAM	CDF	FA [a]	None	*In vitro*: cervical cancer (HeLa), ovarian cancer (SKOV3)	48
SPIO (T_2 MRI) with Cy5.5 for fluorescence	G3.5 PAMAM	PTX	FA [a]	pH-responsive (ester bond)	*In vitro*: breast cancer (MCF-7), hepatocarcinoma (H22) *In vivo*: hepatocarcinoma (H22 s.c.)	51
SPIO (T_2 MRI)	G1/G2	Quercetin	N/A [a]	pH-responsive	*In vitro*: prostate carcinoma (DU145)	52
SPIO (T_2 MRI)	G2.0 Dendritic linear triblock copolymer (PAMAM-*b*-PDMAEMA-*b*-PPEGMA)	DOX	N/A [a]	pH-responsive	*In vitro*: cervical cancer (HeLa)	53
SPIO (T_2 MRI)	G2.0 Dendritic linear triblock copolymer (PAMAM-*b*-PDMAEMA-*b*-PNIPAM)	DOX	N/A [a]	Temperature-responsive	*In vitro*: cervical cancer (HeLa)	54
SPIO (T_2 MRI)	G1/G2/G3 Dendritic linear block copolymer (linear poly(ε-caprolatone), dendritic polyamino-ester and linear PEG)	Quercetin	N/A [a]	pH-responsive		59
SPIO (T_2 MRI)	Peptide dendrimer	DOX and AMF	N/A [a]	None	*In vitro*: cervical cancer (HeLa), HeLa contaminant (KB), breast cancer (MCF-7), prostate cancer (PC-3)	60
SPIO (T_2 MRI)	G2/4/6 dendriplex	Gene therapy (plasmid DNA)	N/A [a]	None	*In vitro*: fibroblasts (NIH 3T3)	64
SPIO (T_2 MRI)	G5 PAMAM dendrimer	Gene therapy (antisense strategy using oligonucleotide)	*Survivin* gene [a]	None	*In vitro*: breast cancer (MCF-7, MDA-MB-435), liver cancer (HepG2), prostate cancer (LNCaP), promyelocytic leukemia (HL-60)	68
SPIO (T_2 MRI)	PPI G5 dendrimer	Gene therapy (siRNA) and cisplatin	LHRH peptide [a]	None	*In vitro*: lung carcinoma (A549; LHRH positive), ovarian cancer (SKOV-3; LHRH negative) *In vivo*: lung cancer (A549 s.c.)	74
SPIO (T_2 MRI)	G4 PAMAM dendrimer	Gene herapy (siRNA)	N/A [a]	None	*In vitro*: breast cancer (MCF-7)	77
SPIO (T_2 MRI) and fluorescence tracking of (EGFR) expression	G4	Gene therapy (siRNA)	Passive [a]	Convection-assisted delivery	*In vitro*: cervical cancer (HeLa) *In vivo*: glioblastoma (GBM-6, transgenic model)	78
Gd(III) (T_1 MRI)	G5 PAMAM dendrimer	DOX	FA	None	*In vitro*: HeLa contaminant (KB)	88
Gd(III) (T_1 MRI)	Dendrimersomes	PLP	Passive	None	*In vitro*: melanoma (B16.F10) *In vivo*: melanoma (B16.F10 s.c.)	90
Gd(III) (T_1 MRI)	G3 dendrigraft poly-L-lysines	Gene therapy	N/A	None	*In vitro*: pancreatic ductal adenocarcinoma (PaCa-2) *In vivo*: pancreatic ductal adenocarcinoma (PaCa-2 orthotopic)	92
Gd(III) (T_1 MRI)	Supramolecular assembly of Ad-PAMAM, Ad-PEG,CD-PEI	DOX	Passive	AMF	*In vitro*: colorectal adenocarcinoma (DLD-1) *In vivo*: colorectal adenocarcinoma (DLD-1 s.c.)	96, 101
Gd(III) (T_1 MRI) with Cy 5 fluorescence probe	G2 polylysine dendrimer with a silsesquioxane core	Surgery	CGLIIQKNEC, CLTI (peptides)	None	*In vivo*: prostate cancer (PC3-GFP orthotopic)	102
^{19}F MRI	Fluorinated G3 and G6 PAMAM	Rhodamine B as model drug	Passive	pH-responsive	*In vitro*: Chinese hamster ovarian cancer (CHO; phantom) *In vivo*: female B6 mouse	134

[a] SPIO structures are also potent for magnetofection targeting approaches.
EGFR: epidermal growth factor receptor; s.c.: subcutaneous

Following this logic, surface functionalization of SPIO with dendrimer enhances not only its stability and targeting capability, but also its capacity for encapsulating drugs or other specific conjugate ligands. These integrated structures possess multiple therapeutic potentials for killing cancer cells via induced magnetic hyperthermia using AMF, controlled drug delivery using pH and temperature, or gene therapy through gene delivery. Altogether, the dendrimer-SPIO complex could serve as a powerful therapeutic platform for simultaneously detecting and treating malignant tumors. The following two sections (section 2.1.1 "Chemotherapy" and 2.1.2 "Gene therapy") are devoted to the advancement and importance of these structures, and their relevant theranostic uses for eliminating the common problems of conventional therapies.

2.1.1. Chemotherapy

A major drawback encountered in traditional chemotherapy is the development of high resistance to the free drug in cancer cells. Often, a very high dose of medicine is required to target and significantly degrade the cancer cells, as traditional chemotherapy relies predominantly on passive targeting and does not show significant EPR effect. The non-specific administration of such a high dose naturally affects healthy cells adversely. For example, breast cancer cells can develop resistance to the commonly used cancer drug doxorubicin (DOX) via Pgp-mediated efflux proteins that prevent drug uptake. As a free drug, DOX often exhibits cardiotoxic side effects [33]. Khodadust *et al.* [34] have shown that polyinosinic:polycytidylic acid (poly I:C)-modified G4 dendrimer-coated SPIO nanoparticles (PIC-G4DcMNP-DOX) could overcome this resistance and deliver DOX inside cancer cells to induce high cytotoxic effects. These authors performed a comparative study of DOX loading, release, and biocompatibility profiles on different generations of PAMAM dendrimer-coated SPIO structures, and found that G4 dendrimers were the most effective for both delivering DOX at a lower pH and overcoming the DOX resistance mechanism in breast cancer cells [35]. Here, poly l:C served as a moderator to reduce the toxic effects of the surface terminal amine group of the PAMAM dendrimer on healthy cells, while triggering apoptosis in human melanoma, breast cancer, and hepatoma cells [36, 37]. So, a higher concentration of the modified nanovehicles could be administered without causing more damage to the healthy cells. However, this poly I:C is bound to the surface of the dendrimer by a phosphoramide bond, which is cleaved by the overexpressed phosphoramidase enzyme in the tumor cells, resulting in release of poly I:C and catalyzing the release of DOX to induce maximum toxicity inside the tumor cells [34]. The DOX-integrated nanovehicle, PIC-G4DcMNP-DOX, showed a lower half maximal inhibitory concentration, indicating higher cytotoxicity compared to free drug [34]. The IC_{50} for poly I:C was 7 μg mL^{-1} and the IC_{50} for DOX was 12 μg mL^{-1} in this integrated complex PIC-G4DcMNP-DOX, whereas free DOX and free poly I:C showed IC_{50} of 170 μg mL^{-1} and 450 μg mL^{-1}, respectively, when tested at 1 μM in DOX-resistant MCF-7 cells. Therefore, a lower dose of DOX could be administered to induce an equal amount of cytotoxic effect to the malignant cells.

The nanoparticle also showed pH-controlled drug delivery functionality and the drug was released more efficiently at a lower pH. The presence of SPIO within the complex PIC-G4DcMNP-DOX could further be used to target specific cancer cells by magnetofection, as described before. Undoubtedly, the poly I:C-modified and drug-loaded G4 PAMAM dendrimer would be preferable over free drug treatment for effective targeting and induction of cytotoxic effects in MCF-7 breast cancer cells, while minimizing adverse effects to healthy cells. However, there is a chance that the phosphoramide bonds may break in tissues other than at the tumor site, as earlier works found a small amount of phosphoramidase enzyme in most healthy tissues. So, a detailed further study is required to understand this mechanism to improve the drug delivery and targeting efficiency.

Pancreatic stellate cells (PSC) activate fibrotic stroma, which strongly resists drug molecules from entering the cancerous cells. As one can imagine, this high resistance places pancreatic cancers as the third leading cause of cancer-related deaths in 2016, as reported by pancreatic cancer action network. A high dose of free gemcitabine could still kill these cancer cells; however, drug administration has to be restricted for its toxic consequences on healthy cells. This problem was addressed by Yalcin *et al*. [38] using an effective dendrimer-based nanovehicle for an active targeting approach. The authors have shown that gemcitabine could be delivered to pancreatic cancer cells using an all-*trans* retinoic acid (ATRA)-conjugated dendrimer-coated SPIO as a nanovehicle. PSC activation of fibrotic stroma is associated with loss of retinol-containing droplets in the cytoplasm [39]. ATRA could be a potential drug to deactivate PSC and overcome the resistance of fibrotic stroma. This dendrimer-based nanovehicle could potentially not only overcome the resistance of fibrotic stroma, but also deliver the required lower dose of gemcitabine to the cancer site, thus minimizing the unwanted side effects. Here, the

authors have taken the advantages of the dual mechanisms of (i) gemcitabine as an anti-cancer drug, and (ii) ATRA to deactivate PSC. However, a previous study using a combination of free retinoic acid and gemcitabine did not show any appreciable improvement in response rate, although these combinations were well tolerated by the patients [40].

On the positive side, this study demonstrated an effective drug-loaded delivery system using an optimized *in vitro* protocol [38]. They have shown that a dendrimer-SPIO nanoparticle, loaded with 10 μM of both gemcitabine and ATRA in PBS buffer at pH = 4.2 released 72% of the drug and 81% of the ATRA within the first 10 h. This released combination was found to be capable of destroying various types of pancreatic cancer cells, including SU86.86, T3M4, and Panc-1 effectively. Although this experiment was performed *in vitro*, it is expected that the therapeutic efficiency would increase considerably when using a delivery nanovehicle as opposed to administering the combination of free drugs.

A major challenge for the successful use of theranostic particles is active targeting, while magnetofection and passive targeting have their own limitations. The advantage of dendrimer over other materials is its ability to bind to a wide variety of specific targeting ligands. Human carcinoma cells in the breast, ovary, endometrium, kidney, lung, head, neck, and brain are known to express folic acid (FA) receptors [41, 42]. Chang *et al.* [43, 44] have shown that SPIO coated with FA and polyethylene glycol (PEG)-conjugated PAMAM dendrimers could be used to selectively target those cancer cells that express FA receptors as well as to enhance the circulation time in the blood for better passive targeting. DOX could be loaded into the dendrimer segment using a hydrazone bond. This bond is sensitive to acidic environments, and has been shown to be capable of 75% drug delivery at pH = 5.03, but has less than 8% delivery at pH = 7.38 [43]. This controlled delivery approach would use a minimum amount of drug, thus reducing the undesirable side effects on nearby healthy cells.

Many anti-cancer drugs have poor solubility in water and are difficult to administer to patients. These anti-cancer drugs could be loaded inside dendrimer-based nanovehicles and administered to achieve much better targeting to the tumor site and efficient drug delivery. For example, 3,4-difluorobenzylidene curcumin (CDF) was reported to have high anti-cancer activities for ovarian, pancreatic, cervical and lung cancers, but suffers from poor solubility [45–47]. Recently, Luong *et al.* [48] showed an effective approach to deliver the hydrophobic anti-cancer drug CDF using FA-PAMAM dendrimer with a SPIO core. Additionally, this approach of loading CDF in FA-PAMAM dendrimer provided higher targeting efficacy, anti-cancer activity, and superior MRI contrast-enhancing ability. Thus, it opens up the possibility of loading other hydrophobic drugs to achieve better targeting and effective therapy of folate receptor-expressing cancers.

Paclitaxel (PTX) is another effective drug used for treating breast cancer, advanced ovarian carcinoma, lung cancer, head, neck, and acute leukemia, but suffers from poor water solubility [49, 50]. In order to effectively administer such drugs, a similar packaging technique could be used. The anti-cancer drug PTX was put inside SPIO-coated dendrimer conjugated to FA, PEG, and cyanine 5.5 (Cy5.5) and then administered [51]. This dendrimer construct is water-soluble and showed high cellular uptake. Since the drug is bound by a cleavable ester bond, the acidic pH environment within tumor cells caused release of the drug, resulting in enhanced cytotoxic effects of PTX. Compared to the non-targeted conjugates, the uptake of the construct was verified using *in vitro* cell fluorescence analysis of a transfected human breast cancer cell line MCF-7. Davayani *et al*. have used a poly(amino ester)-coated SPIO-encapsulated G1 and G2 dendrimer for pH-sensitive drug delivery for prostate cancer [52]. This structure can carry hydrophobic drugs. The authors completed a comprehensive comparison of different functional groups on the dendrimer surface like OH and NH_2. *In vitro* studies using a human prostrate carcinoma cell line revealed that the drug release rate at 37 °C is significantly higher at pH = 5.8 compared to that at pH = 7.4 in standard physiological condition. This change is attributed to a conformational change due to the presence of amino groups in the backbone. Surface-conjugated amino dendrimers showed higher drug encapsulation but slower drug release behavior compared to hydroxyl-conjugated ones. A cytotoxicity assay showed the biocompatible nature of the nanostructures. The efficacy and drug encapsulation could be increased by using a higher generation dendrimer.

Dendritic linear block copolymer modified with SPIO was used recently as an integrated theranostic structure [53, 54]. These structures could be made by combining "grafting onto" [55] and "grafting from" [56] techniques that make SPIO water-soluble, biocompatible, and monodisperse to prevent their aggregation [53, 54]. The polyamidoamine-*b*-poly(2-(dimethylamino)-ethyl methacrylate)-*b*-poly(poly (ethylene glycol) methyl ether methacrylate) (PAMAM-*b*-PDMAEMA-*b*-PPEGMA)-grafted SPIO

dendrimer is capable of carrying and delivering drugs by fine-tuning the hydrogen-bonding interactions between PDMAEMA and DOX [56, 57], making it a pH-sensitive controlled drug delivery system [53]. Studies on these materials showed that the cumulative drug release was maximum within 48 h at pH = 4.7 (83.1%), compared to that at pH = 7.4 (64.7%), and pH = 11.0 (8.3%) at 37 °C [53]. A similar structure was made using the two-step atom transfer radical polymerization (ATRP) procedure with a SPIO core and a dendritic linear-block copolymer with a focal point polyamidoamine-type dendron-*b*-poly(2-dimethylaminoethyl methacrylate)-*b*-poly(N-isopropylacrylamide) (PAMAM-*b*-PDMAEMA-*b*-PNIPAM) shell [54]. This structure showed different amounts of drug release at 25 °C and 37 °C, indicating thermosensitive control of drug release that was attributed to a conformational change of PNIPAM block chains [58]. Another interesting approach along this line is the synthesis of amphiphilic linear-dendritic-linear block copolymers made of a poly ε- caprolactone linear block, poly(amino-ester) dendritic block, and an m-PEG linear block. Oleic acid-coated SPIO was conjugated with G1, G2 and G3 dendrons via a ligand exchange method and *in vitro* pH-guided drug delivery was demonstrated [59].

Most of these dendritic structures were made of PAMAM dendrimer that suffers from the issue of toxicity from its degradation products, which inhibits its clinical use from a safety perspective. Recently, Nigam *et al.* [60] have shown the use of a peptide dendrimer whose core was made of ethylene diamine, and cationic amino acid was taken as the branching monomer. This class of dendrimer is called peptide dendrimer due to the resemblance of the amide linkage between amino acids with the peptide bonds between proteins. Here, the cells utilize amino acids as a nutrient in their metabolism and reduce the toxicity effect after degradation. This could be a potent candidate to solve the long-standing biocompatibility and safety challenges of dendrimer nanoparticles. This peptide dendrimer was loaded with SPIO for MRI detection and co-loaded with anti-cancer drug DOX for therapy similar to other approaches discussed before [60]. Moreover, a combination of DOX and magnetic hyperthermia effect with AMF has been shown to be effective for treating cervical cancers with this nanovehicle [60].

2.1.2. Gene therapy

Gene therapy could be one of the most effective therapies to treat cancers. However, traditional gene therapy suffers from non-specific delivery that produces adverse side effects on healthy tissues [61]. It involves transfer of a particular gene to the targeted site to replace or silence the malfunctioning one, which is responsible for the diseases. It is a very novel way to treat the disease from the origin itself and a very potent technique. However, certain issues like immunological side effects, insertional mutagenesis, *etc.*, limit the scope of this valuable approach. Recent studies show delivery of nonviral particles could be a safer approach to gene therapy with less side effects [62]. Still, it is quite challenging to find an appropriate carrier to encapsulate the genetic particle, limit its exposure to healthy cells, and pass through the cellular obstructions to deliver genes to the cell nucleus. Moreover, for effective gene therapy, the presence of contrast agent in the carrier is necessary to visualize the process noninvasively.

One common way for this is to unify two kinds of genes in the same probe: therapeutic genes and imaging reporter genes (*e.g.*, transferrin receptor gene [63] for MRI). The imaging reporter genes express contrast agents in the target site that could be imaged for efficient tracking of genetic material. However, these imaging reporter genes suffer from immune response, non-favorable kinetics, and lack of stability and biocompatible nature, thus limiting their uses. Here, nanoparticles offer a promising approach to bypass these problems by encapsulating both the therapeutic genes and the imaging reporter genes, thus opening up the possibility of gene therapy along with real-time monitoring of the tumor site. Nanoparticles like dendrimers provide additional means to conjugate bio-moieties for perfect targeting and to minimize the possibility of interaction of the genes with the outside environment and healthy cells. For example, the electrostatic interaction between positively charged PAMAM dendrimer with negatively charged phosphate backbone of DNA forms a complex that protects DNA from degradation [61]. Higher generations of dendrimers show better transfection efficiency due to weaker electrostatic interactions compared to lower generation ones. In an overall sense, dendrimer offers a composite approach to image and deliver genes simultaneously, minimizing the adverse effects of gene therapy.

Shili *et al*. have reported a nanohybrid system by combining plasmid DNA (pDNA) with SPIO for an effective nucleic acid therapy [64]. The authors functionalized different generations of dendrimers with pDNA and poly(styrene) sulfonate-coated SPIO to provide an integrated structure. They characterized and successfully transfected NIH 3T3 cells. Among the generations 2, 4, and 6, they found the optimal one to be G6.

Antisense therapy is an effective strategy for cancer therapy, where antisense oligonucleotides prevent target RNA translation to protein to inhibit

cellular growth [65]. However, it suffers from poor diffusion across cell membranes and undergoes rapid degradation in the absence of a rational delivery mechanism [66]. These problems could be overcome by using a dendrimer-modified SPIO complexed with antisense survivin oligodeoxynucleotides (asODN) [67, 68], since SPIO-coated dendrimer nanoparticles could protect asODN from degradation enzymes by changing the *in vivo* microenvironment inside the cell for a while [69]. Hence, the asODN-dendrimer-SPIO construct could efficiently deliver the gene and successfully inhibit the growth of cancer cells [68]. Among the different generations of dendrimers, G5 is the most effective one for enhancing gene delivery efficiency and downregulating growth of the malignant cells. The exact metabolism pathway is still under study.

Short interfering RNA (siRNA) is another potent candidate for cancer treatment due to its exceptional specificity and ability to silence expressed genes [70, 71]. However, the low permeability of naked siRNA and unavailability of a nontoxic stable nanovehicle for delivery limit its potential applicability [71–73]. Recently, Taratula *et al.* [74] have shown that a poly(propylene imine) (PPI) G5 dendrimer-modified SPIO could solve this problem. They used Luteinizing Hormone-Releasing Hormone (LHRH), whose receptor is overexpressed in many cancer cells, as a specific targeting agent [75]. LHRH-conjugated SPIO-PPI G5-siRNA enhanced the stability and successfully delivered siRNA to the malignant cells. Furthermore, the use of LHRH in the construct enhanced the efficacy of anti-cancer drugs such as cisplatin by suppressing the negative effects on healthy cells [76]. Similar approaches to treat cancers with siRNA have been attempted with G4 PAMAM dendrimer-coated aminosilane-modified SPIO [77]. This kind of structure could overcome the resistance against DOX by breast cancer cells. Another report [78] studied a dendrimer-conjugated fluorophore-labeled magnetic core to internalize siRNA by activating endosomal escape siRNA. The authors successfully showed that different doses of siRNA could be delivered into the cells using the dendrimer-conjugated magnetic nanoparticle, "dendriworms". The dendriworms were delivered *in vivo* to the transgenic glioblastoma mouse model via convection-assisted delivery. This approach offers a route to penetrate the cell cytoplasm freely, resulting in efficient delivery of intact functional siRNA to cells. Furthermore, the use of magnetic nanoparticles and fluorophores opens up the potential of multimodal tracking of siRNA to achieve maximum efficacy of such treatment. While this work focuses on the theranostic applications of the MRI-guided dendrimer-based nanovehicles, the readers can find well-written review articles that comprehensively address the development of gene therapy [61, 79–81].

2.2. Other T_2-mode dendrimer nanoparticles

SPIO holds great promises for futuristic nanomedicine. However, in biological fluids or during exposure to magnetic fields, they sometimes suffer from aggregation and decreased dissolution rates [82]. Commonly used SPIO contrast agents require nonspecific uptake by mononuclear phagocytes to improve the local contrast, and at a hydrodynamic size of over 50 nm, these particles have very limited extravasation ability and are subject to easy uptake by the MPS, which severely undermines their targeting specificity [83]. Hence, the synthesis of biocompatible ultrasmall iron oxide nanoparticles capable of targeting tumor sites could alleviate such concerns, although the preparation of ultrasmall nanoparticles with sizes less than 10 nm is challenging. Recent progresses in this area include efforts [9, 83–85] to prepare the nanoparticles, such as cyclic arginine–glycine–aspartic (RGD) peptides-coated stable iron oxides with 8.4 nm diameter [83]. The RGD coating provides targeting capability to various tumor cells with overexpressed $\alpha_V\beta_3$ integrin [86, 87]. Yang *et al.* [84] incorporated ultrasmall iron oxide nanoparticles inside RGD-coated dendrimers to target brain tumor (C6 glioma cell line) in mice. They showed specific targeting of C6 cells are possible using this nanoparticles. The dendrimer coating imparts extra stability and biocompatibility to the ultrasmall iron oxide nanoparticles and dendrimers provide means for drug delivery and targeted therapy. Future comprehensive studies for drug delivery and other kinds of therapies with dendrimers hold great promise for cancer theranostics.

2.3. T_1-mode dendrimer nanoparticles

Gd-based dendrimers are another class of potential candidates for theranostic uses in association with MRI techniques. Gd(III) is an effective contrast agent [8] that dramatically increases the longitudinal relaxation rate to exhibit positive contrast between malignant and healthy tissues. Similar to the approaches discussed in Section 2.2 for SPIO, theranostic nanovehicles have been designed with Gd(III) as a T_1 contrast agent, instead of SPIO as a T_2 contrast agent. For example, generation 5 amine-terminated PAMAM dendrimer was modified with a Gd-chelate complex (DOTA(Gd)) and targeting ligand FA with PEG to target cancers overexpressing FA receptors [88]. Later, terminal amines were acetylated and the anti-cancer drug DOX was loaded successfully to treat cancer cells simultaneously with

this construct G5. NHAc-DOTA(Gd)-PEG-FA/DOX. Other specific approaches include the use of self-assembled particle dendrimersomes [89], which have been tested *in vivo* for the first time for theranostic uses very recently [90] with the anti-cancer drug prednisolone phosphate (PLP) on murine melanoma mouse models. This work demonstrated an inexpensive and easy alternative to liposome for theranostic purposes [91]. Also, Gd(III)-based dendritic nanoparticles were developed recently for specific targeting in gene therapy under MRI guidance [92], as targeting efficiency has remained a problem in gene delivery systems, as discussed in the previous section. We will summarize two novel directions of Gd(III) nanoparticles in the following Sections 2.3.1 and 2.3.2.

2.3.1. Supramolecular nanoparticle assembly for contrast enhancement and therapy

Gd (III)-incorporated dendrimers could increase contrast in MRI. However, the poor water accessibility to the buried Gd (III) core decreases its relaxation rate, resulting in an overall decreased MRI contrast [93]. To overcome this problem, a porous structure could be used to balance these two opposing effects to make a better contrast agent [94, 95]. Chen *et al.* [96] designed a supramolecular nanoparticle assembly (SNP) of three molecular building blocks consisting of adamantane (Ad)-grafted PAMAM, β-cyclodextrin (CD)-grafted branched polyethylenimine (PEI), and Ad-grafted PEG, which is capable to chelate with a high concentration of Gd(III).DOTA. This structure would provide a pseudo-porous, polymer-dendrimer hydrogel network with good water accessibility. This nanostructure Gd(III).DOTA⊂SNP could be designed to fine-tune the two opposing contrast effects by the systematic variation of SNP size and degree of crosslinking between the materials. Our group and collaborators have shown that the highest relaxivity could be found when Ad-PAMAM and DOTA-CD-PEI exist at a ratio of 1:2, with a Gd(III) concentration of 3.9 mM in the Gd(III).DOTA⊂SNP assembly. Compared to the clinical Gd(III).DTPA complex, which exhibits an r_1 relaxivity of about 4.0 mM^{-1} s^{-1} at 600 MHz, Gd(III).DOTA⊂SNP has shown a remarkable 4-fold increase in r_1 relaxivity of 17.3 mM^{-1} s^{-1} at 600 MHz [96].

This enhanced contrast could be applied for dynamic monitoring of lymphatic drainage, which should be a very useful diagnostic tool for tracking cancer metastasis. Imaging of axillary lymph nodes to observe the lymphatic drainage system could be used as an important diagnostic protocol for breast cancer, as most of the lymphatic fluid from the breast depletes there [97]. It has been shown using *in vivo* mice model experiments that the use of Gd(III).DOTA⊂SNP increases imaging clarity dramatically, in comparison to the conventionally used Gd(III).DTPA [96]. **Figure 3** shows the advantages of using Gd(III).DOTA⊂SNP over Gd(III).DTPA for imaging different lymph nodes with various parameters to obtain the best contrast in MRI. The plot of the average intensity versus time (**Figure 4**) shows the highest clarity for seeing axillary and superficial nodes 80 min after injection of Gd(III).DOTA⊂SNP. Altogether, an effective protocol for early tumor detection comprised the following parameters: time of retention, 150 ms and 50 ms; time of echo, 10 ms; and time after injection, 80 min. Imaging of Gd(III).DTPA in the mouse hand (**Figure 3B**) shows an initial high concentration of Gd(III).DTPA at the injection site 10 min after administering the injection, which dissipates after a short time, suggesting quick clearance of this conventional complex from the body. In contrast, the longer-lasting uniform distribution seen after Gd(III).DOTA⊂SNP injection (**Figure 3A**) implies that this nanovehicle is capable of circulating in the body for a longer period of time. This difference in clearance might be attributed to the difference in the sizes of the nanoparticles.

This structure could be used not only for improving imaging quality, but also for a variety of treatments. For example, gene delivery [98, 99], photothermal treatment [100], and induced hyperthermia [101] could all be achieved using this new complex, classifying it as a potent candidate for theranostic applications. Recently, similar structures with SPIO have been synthesized as AMF-controlled drug delivery nanovehicles for optimized *in vivo* treatment protocols [101]. The study showed that the DOX-loaded nanovehicles have increased cytotoxic effects under AMF, enhancing the antitumor efficacy in comparison to the treatment without AMF [101]. A schematic representation of this procedure is shown in **Figure 5**. The use of this complex allows for the current dosage of DOX to be reduced by a factor of at least 1000, dramatically reducing potential side effects in comparison to traditional protocols.

2.3.2. Image-guided surgery

Real-time detection and monitoring of the tumor during surgery could be an effective alternative to chemotherapy or other types of therapy, by minimizing the possibility of unwanted side effects on nearby healthy tissue. Tan *et al.* [102] performed such image-guided surgery with the help of a dual-modal imaging probe (MRI and cyanine 5 (Cy5) fluorescence imaging) using G2 dendrimer conjugated with CLT1 peptide and loaded with Gd(III)-DOTA monoamide.

This technique could be very effective for detecting and removing prostate cancer, because CLT1 is a cyclic peptide that preferentially binds to fibronectin, which is overexpressed in malignant prostate tissues compared to benign tissues [103–105]. This novel structure exhibited a signal-to-noise ratio 2-fold higher than that of the control agent in MRI, allowing for more accurate detection [102]. Cy5 provides additional bright fluorescence to help determine the precise position of the tumor. Targeting with a small molecular CLT1 peptide, instead of an exogenous monoclonal antibody, reduces the overall dose of the therapeutic and minimizes the potential of inducing a negative immune reaction. This size of the probe allows easy removal of the nanoparticles from the body via renal filtration, making it safe for biological applications. However, the nanostructure suffers from non-specific accumulation in the lung due possibly to either the relatively large size of the agent or the presence of free peptide [102]. Similar nanostructures with lower molecular weight might help overcome this problem. Further study is required to optimize the nanostructure to reduce non-specific tissue accumulation.

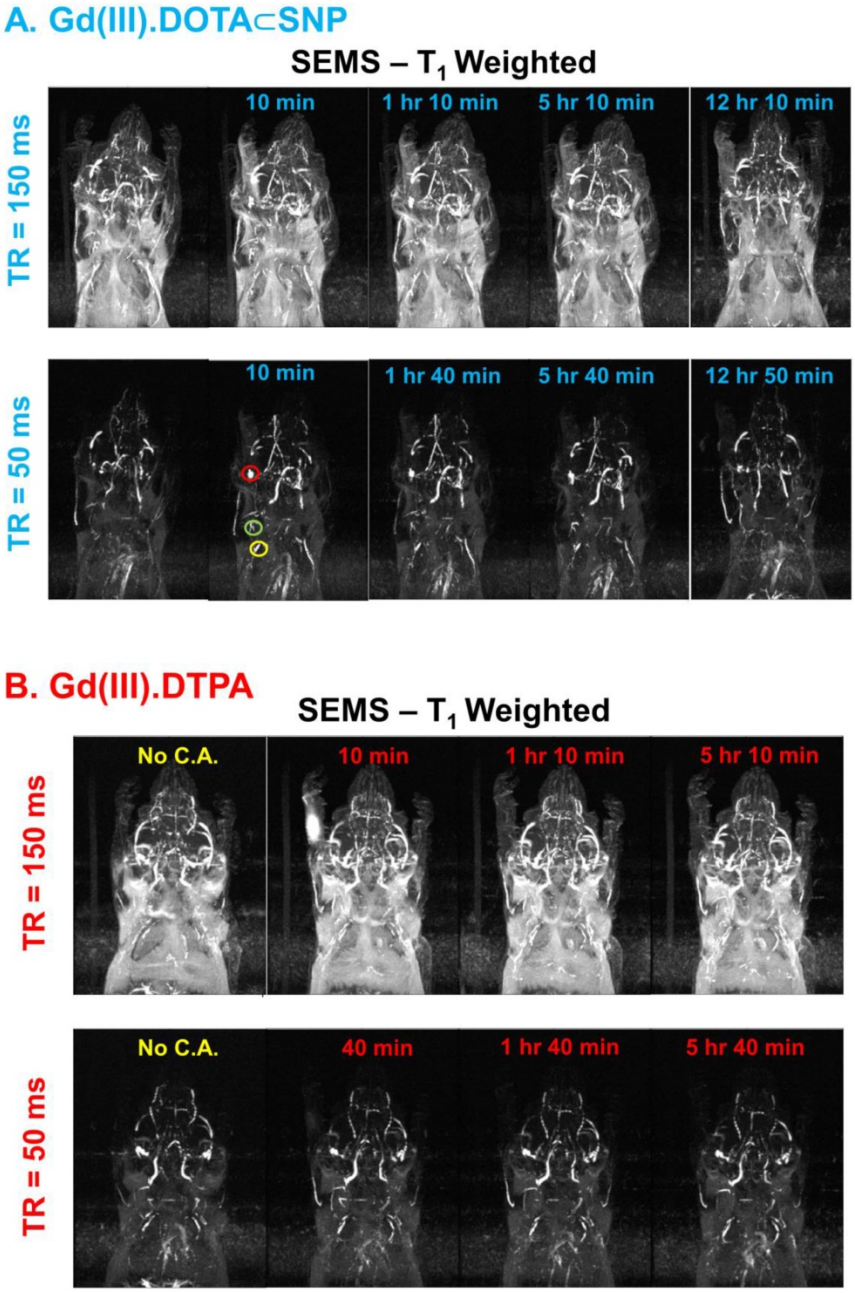

Figure 3. Comparison of MR images of lymph nodes in mice. **(A)** MR images of lymph nodes after injection of Gd(III).DOTA⊂SNPs at different time points under time of retention (TR) 150 ms and 50 ms and time of echo (TE) 10 ms. Red, green, and yellow circles represent the brachial, axillary and superficial lymph nodes, respectively. **(B)** MR imaging of the lymph nodes after injection of Gd(III).DTPA at different time points with time of retention 150 ms and 50 ms, where (A) shows superior contrast at TR = 50 ms.

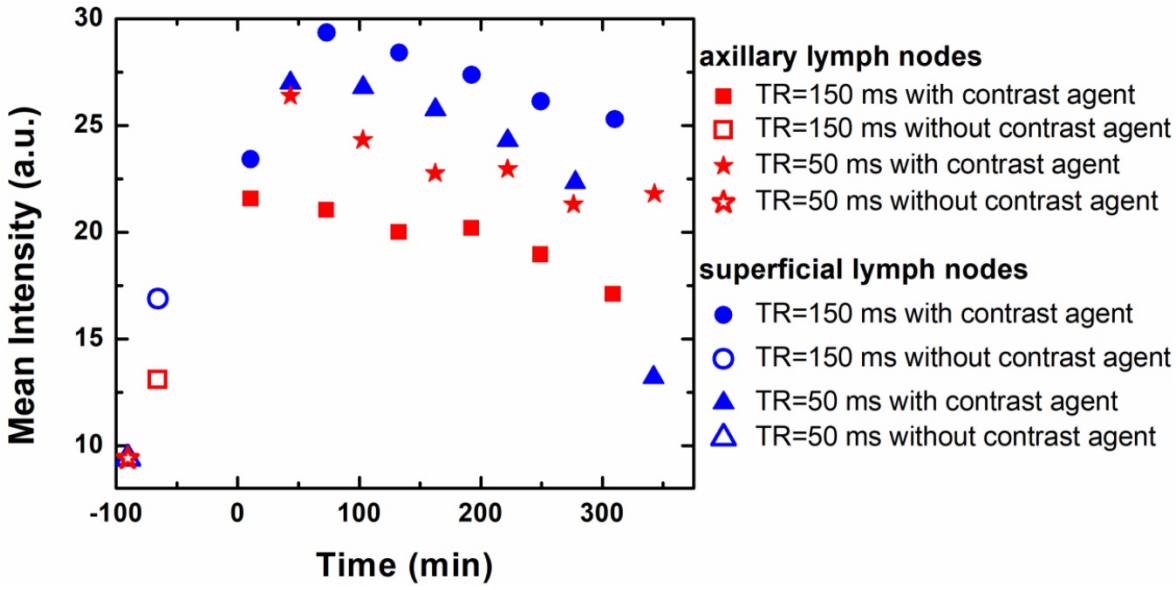

Figure 4. Plot of intensity vs. time after injection of SNP, which shows that the mean intensities of axillary and superficial nodes are highest 80 min after injecting Gd(III).DOTA⊂SNPs.

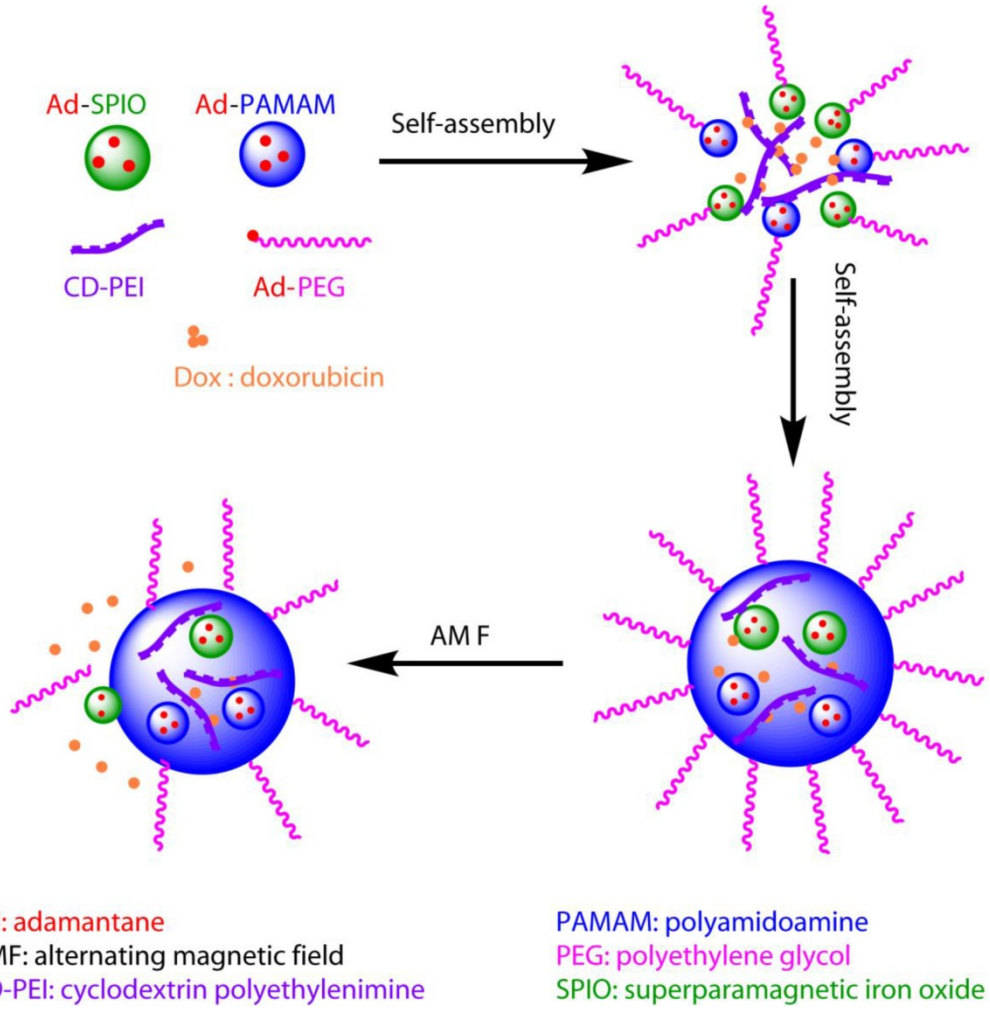

Figure 5. Schematic diagram of the theranostic application of a supramolecular nanoparticle assembly for induced hyperthermic treatment. The diagram shows that drugs (represented by small red balls) can be loaded during assembly of supramolecular nanoparticles, delivered to the tumor site, and released under AMF, which is controlled externally.

2.4. Other T_1-mode dendrimer nanoparticles

Gd(III)-based dendrimers show promise as T_1 theranostic agents in MR. However, Gd has serious side effects called nephrogenic systemic fibrosis [106], especially for patients with renal problems. Although encapsulation of Gd should reduce adverse side effects, other alternatives have been explored. As an alternative, contrast agents based on Mn(II) have been developed [107–112], which could provide reasonable contrast in MRI and are expected to be much safer for patients with renal disease. For example, Zhu *et al*. synthesized a dendrimer-based contrast agent with $[Mn(EDTA)(H_2O)]^{2-}$ [113]. It was characterized and high relaxivity was observed. Its pharmacokinetic properties were evaluated and compared with $[Gd(DTPA)(H_2O)]^{2-}$ in mice. Its blood clearance was observed to be fast and excretion occurred through both the renal and hepatobiliary routes. Hence, it offers an alternative route for imaging patients with impaired renal function. Other recent promising approaches in this direction include the stacking of Mn(II) on negatively charged PEGlyted G2 dendrimer [114]. This nanoconstruct offers high specificity, sensitivity, and capacity to target cancer cells. The authors demonstrated *in vitro* application to the breast tumor cell line MCF-7. As an alternative to Gd-DOTA, Mn(II)-DOTA chelates were synthesized and conjugated with different generations of lysine dendrimer [106, 115]. These Mn-DOTA dendrimers were targeted with CLT1 peptide and studies were performed on breast tumor mouse models. Further studies are required on these kinds of Mn(II)-based dendrimer nanoconstructs to evaluate their applications for therapy, drug delivery, and imaging. They could turn out to be safer and useful theranostic agents for patients with renal disease. Interesting studies on Mn(II)-based dendrimers have been performed in T_1/T_2 and multimodal imaging, as will be discussed below.

2.5. Multimodal dendrimer nanoparticles

We have discussed the development of dendrimer nanoparticles for simultaneous detection and treatment of cancer using MRI in this review. However, multimodal imaging could provide better accuracy and more efficient detection of small tumors compared to single-modal techniques [116, 117]. A lot of research has been done on dual-mode T_1- T_2 imaging using MRI. Such dual-modal imaging [118] would enable us to study both the soft tissue anatomy and pathological phenomenon simultaneously, leading to potential differentiation between normal and tumor tissues, early tumor detection, and prediction of cancer stages [119]. Very recently, Haribabu *et al*. have shown [119] an effective dual-modal approach by encapsulating manganese ferrite nanoparticles [120, 121] in dendrimer and targeting it to tumor by FA. Here, iron served as a T_2 contrast agent and manganese as a T_1 contrast agent. The authors characterized different ratios of Fe-Mn conjugates and found the molar ratio of 0.5 worked best, giving $r_2/r_1 = 4.6$ at a magnetic field of 1.5 T. These kinds of structures could serve as potent theranostics for cancer treatment. However, drug delivery and other pharmacokinetic parameters should be evaluated in future studies.

Other approaches include combinations of different imaging techniques like CT, PET, and fluorescence imaging with MRI. Each imaging modality has its own advantages and disadvantages. For example, MRI enjoys the ability of deep penetration, superior resolution, and non-invasive detection. However, MRI suffers from poor contrast and sensitivity, which could be compensated by PET or SPECT, which have excellent contrast and sensitivity but low resolution. Similarly, CT provides better spatial resolution, and optical imaging such as fluorescence imaging, gives high sensitivity. Hence, combinations with other imaging modalities could potentially overcome the shortcomings of MRI techniques. Examples of such promising directions include the use of entrapped gold (Au) nanoparticles with Gd(III) chelate inside dendrimer for CT and MRI dual-modal detection and targeted therapy [122–125]. This kind of approach was further modified with a SPIO and Au nanoparticle composite for simultaneous CT and MRI detections [126].

Recently, Luo *et al*. [127] have shown a nanocomposite FA-conjugated dendrimer with Mn(II) and Technetium-99m (^{99m}Tc) for targeted therapy and detection with MRI and SPECT. In this method, MRI provided the high spatial resolution, whereas SPECT gave information regarding the physiological condition of the tumor. Furthermore, the use of Mn(II), instead of Gd(III), made it potentially less toxic. A combination of MRI with fluorescence imaging technique to overcome the low sensitivity of MRI could be another useful theranostic approach [45, 78, 102, 128, 129]. As dual modality is better than single modality, tri-modal imaging could work even better compared to dual-modal imaging. Recently, Chen *et al*. [130] have shown that dendrimer functionalized with a nanocomposite of Au nanoparticle, Gd (III), and cyanine dye (Cy5.5) could serve as a tri-modal imaging agent for CT (Au nanoparticle), MRI (Gd(III)), and fluorescence imaging (Cy5.5) to provide better spatial and density resolutions with high sensitivity. Such integrated multimodal theranostic approaches undoubtedly hold great promise for futuristic nanomedicines.

2.6. Heteronuclear dendrimer nanoparticles

In magnetic resonance, "heteronuclear" generally refers to spins other than ^{1}H. For example, the fluorine isotope ^{19}F is a naturally abundant element, and could be used for MR imaging in the place of ^{1}H MR. However, due to its smaller longitudinal relaxation rate (r_1), the imaging quality and sensitivity are limited. A highly dense grouping of ^{19}F is required to produce a strong MRI signal. Typically, the dendrimers are directly synthesized. However, the synthesis of increasingly complex and larger dendrimers demands more challenging approaches, where self-assembly provides an inexpensive alternative [131–133]. Criscione *et al.* [134] have shown a creative approach by self-assembling a ^{19}F probe using a partially fluorinated PAMAM dendrimer. This probe exhibited a fluorophobic effect where fluorinated molecules became separated and assembled into hydrophobic and lipophobic fluorous phases, followed by self-assembly via forming non-covalent bonds [131, 132, 135]. By incorporating a densely packed ^{19}F complex, the self-assembled structure was able to produce a strong MRI signal *in vivo* [134]. Chemical shift imaging along with ^{1}H MRI showed successful site-specific accumulation of the fluorinated particulates [136, 137], and T_1 relaxation rate showed pH dependence in an *in vivo* setting [134]. These self-assembled fluorinated particulates were further modified with PEG for effective passive targeting by enhancing the circulation time in the blood [134]. The partially fluorinated dendrimer structure exhibited pH-dependent disassembly that was assumed to be induced by the presence of the dispersed amines on the surface. These structural characteristics might enable us to develop an efficient pH-guided drug delivery system in the future.

3. Copolymer-based nanoparticles for MR cancer theranostics

A core-shell nano-platform can be composed of a variety of materials. Although the core is surrounded by a hydrophilic shell, the overall structure is stabilized by either covalent or ionic bonds between the core and shell (**Figure 2**). The physiological stability, surface modification simplicity, drug releasing ability [138], and core and shell component flexibility of core-shell nano-platforms show great promise for theranostic purposes. Here, we aim to present the most recent developments of core-shell nano-platforms formed by copolymers that consist of both hydrophobic and hydrophilic blocks.

The hydrophilic block of the copolymer (*e.g.*, PEG) often serves as the outer shell to provide good water solubility and biocompatibility, ultimately reducing the premature clearance of core-shell nanoparticles, therefore prolonging the circulation time in the blood. Alternatively, the hydrophobic block of the copolymer provides sufficient interactions with the typically hydrophobic anti-cancer drugs to increase the drug or contrast agent loading efficiency. The flexibility of the structure of copolymers enables them to encapsulate, bind, and/or conjugate to therapeutic and/or imaging agents with simple modification procedures, and adapt to various *in vivo* environments. Thus, they are excellent candidates as theranostic nano-platforms as well as coating materials.

3.1. T_2-mode copolymer nanoparticles

3.1.1. Targeting strategy

Most core-shell copolymer nanovehicles take advantage of the above-mentioned EPR effect to passively target and accumulate at the tumor site. Filippousi *et al.* [139] synthesized amphiphilic triblock copolymers of hydrophobic poly(propylene succinate) (PPSu) and hydrophilic PEG. The core-shell magnetic nanoparticles were formed by encapsulating magnetite (Fe_3O_4) and the anti-cancer drug paclitaxel (PTX) into the hydrophobic core. Furthermore, three copolymer samples were prepared with similar lengths of PEG blocks, but with different lengths of PPSu blocks, allowing for further investigation of the effect of the hydrophobic (PPSu) to hydrophilic (PEG) ratio of the polymeric matrix. All three samples exhibited satisfactory nanoparticle yield (ranging from 70.57% to 78.21%) and drug entrapment efficiency (ranging from 53% to 65%). However, the differences in the hydrophobic block among the three samples produced varying drug-release profile patterns in an *in vitro* environment. The copolymer sample of 5800 g mol^{-1} PPSu released approximately 100% PTX loaded within 25 h, while the sample with 18900 g mol^{-1} PPSu had a maximal release of 80% even after 240 h.

A recent study published by Bakewell *et al.* [140] depicts the synthesis of a triblock copolymer mPEG-block-poly[(D-glutamic acid-gamma-hydroxamate)-co-(L-glutamic acid-gamma-hydroxamate)]-block-poly[(L-tyrosine)-co-(D-phenylalanine)]-acetamide and its application as a drug-loaded, iron-stabilized platform. Anti-cancer drugs were loaded in the hydrophobic core, while iron chelates with hydroxamic acid moieties formed dative bonds among polymer stands and stabilized the micelle. In their study, six active pharmaceutical ingredients (API) were loaded individually, resulting in different loading efficiencies (ranging from 65% to 91%) and average diameters of the micelles (ranging from 58

nm to 120 nm). *In vivo* study in subcutaneous xenograft mouse models showed enhanced MRI contrast after injection of the micelles, and increased anti-tumor efficacy compared to free drug.

Schleich *et al.* [141] synthesized PTX/SPIO-loaded PLGA-based nanoparticles by mixing poly(lactide-co-glycolide) (PLGA), poly(ε-caprolactone-b-ethylene glycol) (PCL-b-PEG), (PLGA-PEG), oleic acid-coated SPIO, and PTX through emulsion-diffusion-evaporation. The resulting nanoparticles were composed of a hydrophobic core containing the SPIO and PTX, and a PEG block hydrophilic shell. Such PTX/SPIO-loaded nanoparticles possessed a high r_2/r_1 ratio of 33.4 at 20 MHz, which is higher than that of the conventionally available magnetic nanoparticle Resovist, presenting promising applications as a T_2 contrast agent. Both *in vitro* cytotoxicity studies of CT26 colon carcinoma cells and *in vivo* anti-tumor studies of CT26-tumor-bearing mice showed PTX/SPIO-loaded nanoparticles inhibited the growth of CT26 cells. Based on Kaplan-Meier survival rate analysis, the PTX-load and PTX/SPIO-loaded nanoparticles exhibited superior survival rates, with median survival rates of 13 and 15 days respectively, than the PBS-administered control group with a median survival rate of 9 days.

Even with the same copolymer composition, different conjugated structures will affect drug release characteristics. Wang *et al.* [142] synthesized two similar core-shell nanoparticles using Fe_3O_4-SiO_2: poly(benzyl L-aspartate) (PBLA) and methoxy poly(ethylene glycol) (mPEG). The first core-shell nanoparticle, FeSi@PBLA@mPEG, was synthesized by first conjugating PBLA with Fe_3O_4-SiO_2, then conjugating the methoxy poly(ethylene glycol) benzaldehyde(mPEG-CHO) onto the resulting nanoparticle through benzoic-imine bonds. The second core-shell nanoparticle, FeSi@PBLA-mPEG, was produced in a one-step conjugation of Fe_3O_4-SiO_2 to the diblock copolymer of mPEG-PBLA, where mPEG and PBLA were copolymerized through peptide bonds. Both core-shell nanoparticles were loaded with the anti-cancer drug DOX to form the complexes FeSi@PBLA@mPEG@DOX and FeSi@PBLA-mPEG@DOX, respectively. *In vitro* drug release studies showed that in a PBS buffer solution of pH = 7.4, the drug release profile patterns of the two DOX-loaded core-shell nanoparticles were very similar, both being less than 25% after 50 h. When the buffer was adjusted to an acidic environment of pH = 5.8, the release of DOX from FeSi@PBLA@mPEG@DOX was accelerated and reached 45% after 50 h. In contrast, FeSi@PBLA-mPEG@DOX did not show much difference between the acidic and neutral conditions. This difference in drug release behavior between the two core-shell nanoparticles is mainly attributed to the pH-sensitive benzoic-imine bonds between mPEG and PBLA in FeSi@PBLA@mPEG@DOX.

Active targeting and delivery can be achieved by conjugating active tumor-targeting ligands onto the copolymer shell. A generally used targeting ligand is FA, as it is able to enhance the targeting efficiency of the nano-platform to cancer cells through folate receptor-mediated endocytosis. Yang *et al.* [143] designed a wormlike polymer vesicle using amphiphilic triblock copolymers PEG_{114}-PLA_x-PEG_{46}-acrylate (PLA: poly(D,L-lactide). The short PEG segments of the wormlike vesicles bearing acrylate groups encapsulated clusters of SPIO nanoparticles into the vesicles, while the long PEG segments were bound to FA, offering the vesicles active tumor-targeting ability. The hydrophobic layer PLA was used to load the hydrophobic anti-cancer drug DOX. Folate receptor-mediated endocytosis led to a higher cellular uptake of FA-conjugated wormlike vesicles in the HeLa cell line than FA-free ones, resulting in higher cytotoxicity and increased MRI sensitivity.

Patra *et al.* [144] manufactured core-shell nanoparticles of SPION@PS-b-PAA-DOX/FA with an SPIO core containing a contrast agent encompassed by a poly(styrene)-b-poly(acrylic acid) (PS-b-PAA) shell not only containing DOX for therapy, but also containing FA peripherally conjugated to the outer shell for recognition of the cancer site. Both the drug release profile and magnetization of such core-shell nanoparticles improved dramatically upon altering the neutral physiological pH of 7.4 to an acid pH of 5.3. At pH = 5.3, the nanoparticle revealed an initial burst of drug release from 0% to 37%, reaching a final 92% after 160 h. At pH = 7.4, however, the nanoparticle only had an initial release from 0% to 12%, reaching a final release of 32%. Additionally, the r_2 relaxivity of the nanoparticle at pH = 5.3 was found to be more than 5 times that at pH = 7.4. This result was expected, as DOX is conjugated to the core-shell nanoparticle through a pH-sensitive hydrazine linkage. Further *in vitro* cell viability assays on human breast cancer SkBr3 cells and colon cancer HCT116 cells demonstrated that SPION@PS-b-PAA-DOX/FA had a higher efficacy in killing cancer cells compared to free DOX, mainly because the conjugated drug could be internalized at a higher rate and had longer retention time in the intracellular environment.

Wang *et al.* [145] co-encapsulated both SPIO nanocrystals and DOX into PLGA/polymeric liposome core-shell nanocarriers. The core-shell nanocarrier was self-assembled from a hydrophobic

PLGA core and a hydrophilic FA-coated PEGylated lipid shell. The MRI signal intensity of Hela cells incubated with the FA-targeting magnetic core-shell nanoparticles decreased in T_2-weighted imaging when the Fe concentration in the cells increased, and such trend was more obvious compared to magnetic PLGA sphere or magnetic core-shell nanocarrier without FA coating. The FA-targeting magnetic core-shell nanoparticles also showed greater cell uptake than non-targeting ones *in vitro*.

Ji *et al.* [146] synthesized a hollow, porous Fe_3O_4 ($HPFe_3O_4$) nanoparticle that was loaded with DOX in the cavity, then self-assembled with polymers of [7-(didodecylamino)coumarin-4-yl] methyl methacrylate (DDACMM) and PEG. The complex was then conjugated with FA for selective cancer targeting and was found to be NIR light responsive. The resulting $HPFe_3O_4$@DDACMM-PEG-FA nanoparticles showed continuous drug release under femtosecond pulse NIR laser exposure, with a final release amount of 70% at pH = 5.0, and 50% at pH = 7.4 after 24 h. When placed in the dark, however, less than 10% DOX was released during the 24-h period, regardless of the pH environment. An *in vitro* MTT assay on folate receptor protein-positive human KB FR(+) cells further verified this selective release under NIR exposure. The $HPFe_3O_4$@DDACMM-PEG-FA nanoparticles also possessed a high r_2 relaxation rate of 139.1 Fe mM^{-1} s^{-1}.

Alternatively, cRGD ligand can also serve as a targeting moiety, since it can target $\alpha_v\beta_3$ integrins on tumor endothelial cells. Nasongkla *et al.* [147] synthesized polymeric micelles using amphiphilic block copolymers of maleimide-terminated PEG-block-PLA (MAL-PEG-PLA) and methoxy-terminated PEG-block-PLA (mPEG-PLA). SPIO nanoparticles and DOX were loaded in the hydrophobic core, while cRGD was attached to the surface of the hydrophilic shell. *In vitro* MRI and cytotoxicity studies confirmed the enhanced MRI relaxivity and $\alpha_v\beta_3$-specific cytotoxic response of the cRGD-conjugated polymeric micelles, due to the induced receptor-mediated endocytosis for cell uptake.

Cancer cell antigens are specific structural substances on the surface of cancer cells that can serve as a target for adaptive immuno-targeting. These antigens can be recognized and specifically bound by the corresponding antibody. Through the high selectivity and binding affinity between antibody and antigen, the nano-platform conjugated with antibody on the surface can be used to target corresponding cancer cells with high efficiency and specificity. This has been verified by both *in vitro* and *in vivo* studies of drug-loaded magnetic core-shell nanoparticles conducted by Gao *et al.* [148]. In their study, a core composed of PLGA, the anti-cancer drug DTX, and hydrophobic SPIONs, was first created using a single emulsion evaporation method, then subsequently conjugated with poly(allylamine hydrochloride) (PAH), and two differently sized poly(ethylene glycol) (PEG) molecules through a layer-by-layer strategy. The outer shell PEG molecules were conjugated with prostate stem cell antibody (scAb), for a more specific targeting capability to prostate stem cell antigen-positive PC3M cells. This specific binding was confirmed by an *in vitro* cytotoxicity study of scAb-PLGA-SPIO/DTX (nano-platform conjugated with scAb; DTX: docetaxel) and PLGA-SPIO/DTX (without scAb) on PC3M cells and HT29 cells. For PC3M cells, the IC_{50} of scAb-PLGA-SPIO/DTX was found to be significantly lower than that of PLGA-SPIO/DTX. In contrast, the prostate stem cell antigen-negative HT29 cells revealed IC_{50} values both with or without scAb that were very similar. *In vivo* MRI and antitumor efficacy studies also confirmed the effective targeting of scAb-PLGA-SPIO/DTX to the tumor site. *In vivo* MRI showed significant contrast between tumor and muscle after injection of either scAb-PLGA-SPIO/DTX or PLGA-SPIO/DTX, due to SPIO accumulation at the tumor site via the EPR effect. However, scAb-PLGA-SPIO/DTX showed further contrast enhancement due to the additional antigen-antibody targeting interaction. Furthermore, scAb-PLGA-SPIO/DTX induced long-term tumor inhibition in PC3M tumor-bearing mice and possessed the smallest mean tumor volume of 156.4 ± 12.6 mm^3 (at 75 days) in comparison to the other conditions. Specifically, without the antibody scAb conjugated to PLGA-SPIO/DTX, the tumor volume was found to be 269.9 ± 225.4 mm^3 (at 72 days), free DTX-treated tumor had a volume of about 500 mm^3 (at 57 days), and PBS-treated tumor had a volume of about 750 mm^3 (at 33 days). As described, the copolymer sections in the core-shell nanoparticles provide a variety of functional groups that can bind different targeting moieties for extended applications to other cancer types for specific contrast enhancement and targeted therapy through antigen-antibody interactions.

Another promising active targeting strategy is magnetic targeting (MT). Magnetic targeting enhances accumulation and retention of drug-loaded magnetic nanoparticles in tumors by applying an extra, external magnetic field [149]. Yang *et al.* [150] produced a highly magnetic nanocarrier (HMNC) composed of a Fe_3O_4 core and an aqueous-stable, self-doped poly[N-(1-one-butyric acid)]aniline (SPAnH) shell. The surface of the HMNC was conjugated with the

anti-cancer drug 1,3-bis(2-chloroethyl)-1-nitrosourea (BCNU). To achieve a high BCNU drug loading capacity and a long circulation time *in vivo*, the HMNC was further modified by grafting *o*-(2-aminoethyl)polyethylene glycol (EPEG) to form a self-protecting magnetic nanomedicine (SPMNM). Contrast enhancement and drug delivery efficiency via MT treatment were evaluated using a subcutaneous mouse tumor model. R_2 constant mappings showed an increased R_2 value at the tumor site, reaching the highest R_2 value with a 24-hour exposure of external magnetic field. The R_2 value at the tumor site significantly decreased after 48 h of MT, which the authors attributed to metabolization of SPMNM. The mice that received SPMNM with 24 h of MT treatment also showed a much higher survival rate compared to mice treated with free BCNU or SPMNM alone, with a median survival of 63 days for SPMNM/MT vs. 50 days for free BCNU and 48 days for SPMNM alone. Recent studies by Liao *et al.* [151] and Zhu *et al.* [152] also took advantage of magnetic targeting by applying an extra magnetic field to mediate active targeting of theranostic platforms to the tumor site. In both studies, the strong fluorescence signals of the dual-modal probes confirmed the enhanced targeting under the extra magnetic field.

3.1.2. Triggered release mechanisms

To enhance controlled release of loaded drug, nanocarriers with a triggered release mechanism have attracted great attention in recent years. Core-shell structures that can release drugs in response to specific stimuli such as temperature, pH, and redox conditions have been developed to achieve superior anti-cancer efficacy and minimize drug resistance and side effects. Among these specific stimuli, pH-responsive drug delivery systems have received great attention for their potential applications in selective and controllable drug release at tumor sites. For example, Asadi *et al.* [153] developed a core-shell structure with SPIO core and copolymer shell that is composed of pendant-activated ester moieties, *i.e.*, pentafluorophenyl acrylate (PFPA) and polyethylene glycol monomethyl ether methacrylate (PEGMA). DOX was then loaded onto the copolymer shell. Drug release kinetic study found that the maximum DOX release at pH = 7.4 was about 14 wt%, which increased to 45 wt% at pH = 5.4, and remained higher than 35 wt% within 50 h. Biswas *et al.* [154] synthesized an amphiphilic block copolymer PEG-*b*-P(*t*BMA-co-MAA) (*t*BMA: *t*-butyl methacrylate; MAA: methacrylic acid) consisting of a hydrophilic PEG block and a hydrophobic methacrylate block containing pendant carboxylic acids. The copolymer micelle then encapsulated SPIO nanoparticles into its hydrophobic core, and loaded DOX. In acidic environments, more carboxylic acid groups in the copolymer exist as their neutral forms (COOHs) and therefore exhibit a weaker electrostatic interaction with the amine groups of DOX molecules, resulting in higher DOX release in aqueous solution at pH = 5 compared with pH = 7.4. Feng *et al.* [155] synthesized triblock copolymers of PEG, poly(N-(N',N'-diisopropylaminoethyl) aspartamide) (P(Asp-DIP)), and poly (lysine-cholic acid) (P(Lys-Ca)) (PEG-P(Asp-DIP)-P(Lys-Ca). The copolymer encapsulated SPIO and PTX inside its core in aqueous solution at neutral pH, and disassembled in acidic lysosomal compartments for rapid drug release.

The design of a redox-responsive drug delivery system can be achieved by including disulfide bonds in the copolymer, which can be cleaved via a thiol-disulfide exchange reaction with the reducing agent glutathione tripeptide (GSH). The GSH concentration is relatively low in plasma (2–20 μM), but tumor tissue is highly reductive and shows much higher GSH concentration (~10 mM) [156]. Therefore, the disulfide bonds cannot be cleaved in plasma and disulfide bond-containing copolymers remain stable in blood circulation, while the disulfide bonds are expected to be broken in tumor tissue due to the local high GSH level. As a result, part of the nanocarrier will be detached and the cellular uptake of the nanocarrier will be enhanced in tumor tissue. For example, Yu *et al.* [157] synthesized the graft copolymer mPEG-SS-NH-graft-PAsp-DA, and loaded Fe_3O_4 and DOX to form drug-loaded magnetic nanomicelles. Detachment of the PEG shell in tumor tissue resulting from cleavage of disulfide bonds accelerated release of DOX and enhanced cellular uptake. Ding *et al.* [158] developed a degradable micellar system assembled from multiblock polyurethanes-bearing disulfide bonds throughout the backbone. The copolymers were also bound to gemini quaternary ammonium (QA) pendent groups in the side chain to increase permeability of the micelles across the cell membrane for higher delivery efficiency. SPIO nanoparticles and anti-cancer drug triptolide were loaded into the core of the structure. The micelles exhibited enhanced release of drug within tumor cells, probably because the disulfide bonds embedded in the backbone were cleaved by the high GSH level in the tumor, resulting in destabilization of the micelles.

3.1.3. Gene therapy

Gene therapy uses transgenes to treat diseases and is a promising therapeutic approach for cancer treatment. Effective delivery of gene vectors into the target site is essential in gene therapy. Zhang *et al.*

[159, 160] synthesized nanovectors with an iron oxide nanoparticle core coated with a copolymer of chitosan, PEG, and PEI. Green fluorescent protein-encoding DNA was bonded to the nanovectors to test the gene delivery efficiency. *In vivo* studies on xenograft tumors of C6 glioma confirmed accumulation of the magnetic nanoparticles to the tumor, resulting in an increase of R_2 constant and gene expression, which could be further enhanced if the nanovectors were labeled by chlorotoxin. In their recent work [161], catechol was grafted onto the chitosan backbone of the copolymer shell to increase its affinity to the iron oxide core, and therefore enhanced MR relaxivity and enabled the possibility to fine-tune its physiochemical properties. In cell transfection experiments on the human GBM cell line SF767, the copolymer nanovectors showed high transfection efficiency with minimal cell toxicity.

Wang *et al.* [162] synthesized core-shell micelles using a block copolymer of PLA and mPEG. SPIO nanoparticles were loaded into the cores of the micelles. To effectively load and protect the nucleic acids, the micelles were surface-coated with cationic polymers like chitosan and PEI. A plasmid DNA was loaded onto the core-shell micelles and efficiently transfected various cell lines. Lee *et al.* [163] synthesized magnetic micelles with a SPIO aggregates core and PHEA-g-PEG-bPEI copolymer shell, which was prepared by grafting PEG and PEI blocks onto the poly(2-hydroxyethyl aspartamide) (PHEA) backbone. pDNA was then loaded into the magnetic micelles, and gene transfection was confirmed *in vitro* using the CT-26 colon cancer cell line. Wan *et al.* [164] developed a magnetic theranostic gene delivery system with a SPIO core and a biodegradable stearic acid-modified low molecular weight polyethyleneimine (Stearic-LWPEI) shell. This delivery system showed high minicircle DNA (mcDNA) binding capability, and was able to protect mcDNA from enzymatic degradation and controllably release mcDNA in the presence of polyanionic heparin. Lee *et al.* [165] conjugated human vascular endothelial growth factor (VEGF) siRNA to PEG-PCL copolymer, then prepared micelles by mixing PDMA-b-PCL diblock copolymer with PEG-PCL copolymer. Ultra-small SPIO (USPIO) nanoparticles and the anti-cancer drug 7-ethyl-10-hydroxycamptothecin (SN-38) were then loaded into the hydrophobic core of the PCL block of the micelle. In *in vivo* experiments on mice bearing LS174T human colon adenocarcinoma tumors with high VEGF expression, the SN-38/USPIO-loaded micelles significantly inhibited the growth of tumor, resulting from the synergistic effect of chemotherapy and gene silencing.

3.1.4. Hyperthermia and photothermal therapy

Magnetic nanoparticles can also be used for treatment of cancer through hyperthermia, which is the heating of cells in the range of 41–47 °C [166]. Hyperthermia effect also increases the drug release efficiency at the tumor site. Xie *et al.* [167] synthesized nanoparticles with a Mn-Zn ferrite nanocrystal core and a PEG-phospholipid (1,2-distearoyl-*sn*-glycero-3-phosphoethanolamine-*N*-[methoxy(polyethylene glycol)] copolymers, DSPE-PEG2000) shell. The core-shell structure displayed excellent magnetic and thermal performance (r_2 = 338 mM^{-1} s^{-1}, specific absorption rate SAR = 324 W g^{-1} Fe). When exposed to AMF of 12 A at 390 kHz, the Mn-Zn ferrite nanocrystal core induced heating of the tumor surface to approximately 43 °C 30 min after i.v. injection. To study tumor growth behavior, tumor-bearing mice were treated with four core-shell nanoparticle injections and eight AMF exposures in 12 days. Tumor growth was significantly attenuated compared to that of the control group who received AMF exposure but without injection of core-shell nanoparticles.

It has been noticed that gold nanoparticles with specific shapes display strong surface plasmon resonance absorption intensity in the NIR region, making them potential candidates for photothermal therapy of cancer or other lesions [168]. The past decade has seen an increasing interest in combining Fe_3O_4 and Au nanoparticles for their theranostic potential in MRI contrast enhancement and photothermal therapy. Li *et al.* [169] encapsulated a Fe_3O_4 core with a star-shaped Au shell, and then conjugated PEI and hyaluronic acid on the surface for an outer shell. Photothermal images of tumor-bearing mice injected with the nanoparticles followed by irradiation with a 915 nm laser confirmed a rapid temperature increase at the tumor site from 32.8 °C to 58.9 °C after 90 s laser irradiation, and the local high temperature (above 50 °C) remained for 205 s. Dong *et al.* [170] developed a nanocomposite with a superparamagnetic Fe_3O_4 core, a middle shell of the amphiphilic block copolymer PS-b-PAA, and an outer layer of gold shell. Thermal images showed that during irradiation with an 808 nm laser, the temperature of the tumor region injected with the nanocomposite increased from approximately 35 °C to 60 °C. Chen *et al.* [171] designed a theranostic nanoparticle with an iron oxide core surrounded by a polysiloxane layer and grafted with poly(ethylene oxide). NIR-resonant gold sulfide nanoparticles (Au_2SNPs) were loaded in the shell. Under exposure to an 885 nm laser, the Au_2SNPs nanoparticles generated a significant temperature rise from room temperature to 54 °C, with no degradation of the

photothermal capability observed during repeated laser on/off cycles.

3.1.5. Other T_2-mode copolymer nanoparticles

In addition to iron oxide, MnFe and FePt alloys can also serve as effective T_2 contrast agents. Yang *et al.* [172] synthesized amphiphilic block copolymers, loaded $MnFe_2O_4$ nanocrystals and DOX in the hydrophobic PCL core, and attached the anti-HER antibody (HER, Herceptin) on the surface of the shell. *In vivo* experiments on mice bearing breast cancer showed that the core-shell nanoparticles were able to show superior R_2 enhancement at the tumor site than the passive control using the EPR effect without antibody targeting, and excellent effects for the inhibition of tumor growth. Liu *et al.* [173] encapsulated FePt alloy nanoparticle into Fe_2O_3, and then coated the structure with amphiphilic PEG graft poly(maleic anhydride-alt-1-octadecene) (C_{18}PMH-PEG) polymer. DOX was then loaded into the hydrophobic block of the polymer shell, while FA was conjugated to the hydrophilic part for folate targeting.

3.1.6. Multimodal imaging and combined therapy

Multimodal imaging is the integration of two or more imaging modalities, utilizing the strengths of individual modalities while overcoming their limitations. Fluorescence dyes and MRI contrast agents are loaded/encapsulated in the copolymer carriers/platforms to achieve bimodal imaging of fluorescence and MR. Liao *et al.* [151] encapsulated SPIO, cyanine dye (IR820), and PTX with poly(ε-caprolactone-co-lactide)-b-poly(ethylene glycol)-b-poly(ε-caprolactone-co-lactide) (PCLA-PEG-PCLA) copolymer. NIR fluorescence imaging and MR images of 4T1 tumor-bearing BALB/c mice showed accumulation of the SPIO/IR820-loaded copolymers at the tumor site 8 h after injection. When exposed to an extra magnetic field, the tumor regions were found to have higher fluorescence intensity and lower MR signal compared to images acquired without the extra magnetic field, which also confirmed the efficiency of magnetic targeting.

Zhou *et al.* [174] combined ultrasound with T2-MRI for dual imaging. They designed a nano-platform with perfluorohexane (PFH) microbubbles as the core and PLGA as the shell. Fe_3O_4 nanoparticles were loaded in the shell, DOX was encapsulated in the inner surface of the shell, while FA was conjugated to the outer surface of the shell, and the resulting nano-platform had the structure PFH/DOX@PLGA/Fe_3O_4-FA. The temperature-responsive PFH core enhanced ultrasound imaging contrast and high-intensity focused ultrasound (HIFU) therapeutic efficiency. Compared to the non-targeted group (no FA conjugation on the outer surface of the shell), the designed nano-platform showed superior contrast in T_2-weighted MR images and real-time ultrasound images.

Combined therapy of multiple treatments shows great promise due to synergistic therapeutic effects. Purushotham *et al.* prepared composite nanoparticles of 43 nm γ-Fe_2O_3 nanoparticles coated with PNIPAM [175]. The thermoresponsive polymer shell was then loaded with DOX. *In vivo* magnetic targeting to the tumor with DOX-loaded PNIPAM-iron oxide nanoparticles was studied in a rat model implanted with hepatocellular carcinoma (HCC). MRI and histology showed that the injected nanoparticles were localized in the HCC, which demonstrated the targeting efficiency of the core-shell nanoparticles. The *in vitro* DOX release under magnetic hyperthermia conditions (variable strength of alternating magnetic fields ranges from 0.1–4 kA m^{-1} and a starting temperature of 37 °C) reached 14.7% after a total of 47 min, within which there was 30 min of exposure to hyperthermia temperature (41–48 °C) and 17 min above body temperature (37 °C). Further adjustment on the lower critical solution temperature of PNIPAM can be reached by using appropriate copolymers to achieve better synergistic therapeutic effect. *In vivo* study of the above-mentioned nanostructure PFH/DOX@PLGA/Fe_3O_4-FA [174] also showed that, when combined with HIFU, the inhibition efficiency for tumor growth was notably stronger than that of all control groups (non-targeted, chemotherapy only, HIFU only, free DOX, and saline).

3.2. T_1-mode copolymer nanoparticles

Gd-based and manganese-based [176] contrast agents are commonly used T_1 contrast agents for MRI, and they produce efficient positive contrast enhancement in T_1-weighted imaging. For example, Tong *et al.* [177] designed and synthesized a core-shell nano-carrier using 1,4,7,10-tetraazacyclododecane-1,4,7,10-tetraacetic acid-poly(ethyleneglycol)-block-poly(acrylamide-co-acrylonitrile) (DOTA-PEG-b-poly(AAm-co-AN)). Gd^{3+} ions and DOX were loaded into the hydrophobic core and chelated on the shell during the self-assembly process. *In vitro* experiments showed an elevated r_1 relaxivity of 25.88 mM^{-1} s^{-1}. Moreover, the chelated structure enhanced the cellular uptake efficiency of DOX to 2.12 times that of free DOX.

3.2.1. pH-responsive copolymer nanoparticles

Polyelectrolyte multilayers are promising candidates as a material for the shell of core-shell nanoparticles due to their pH-responsive drug

encapsulation and release. Huang *et al.* [178] first synthesized Gd_2O_3:Yb^{3+}:Er^{3+}, a functionalized mesoporous silica nanoparticle core, which was then coated by multiple layers of polyelectrolyte poly(allylamine hydrochloride) and poly(sodium 4-styrenesulfonate) using a layer-by-layer technique. DOX was then loaded onto the polyelectrolyte shell in a strong acidic condition of pH = 2.0. The resulting DOX-loaded core-shell nanoparticles had an r_1 rate of 7.35 mM^{-1} s^{-1}. While less than 10% DOX was released over a 72 h period in a PBS buffer of pH = 7.4, more than 60% DOX was released within 72 h at pH = 5.2. *In vitro* cytotoxicity studies on MCF-7 breast cancer cells showed that both DOX-loaded nanoparticles and free DOX exhibited high cytotoxicity, although the former exhibited higher cytotoxicity than the latter. However, this enhanced cytotoxicity in the DOX-loaded nanoparticles should not be attributed to the platform itself, as the core-shell nanoparticles without DOX had negligible cytotoxic effects on MCF-7 cells. The authors attributed this enhanced performance to the acidic microenvironment of endosomes and lysosomes, and the weakly acidic extracellular environment at the tumor site, which in turn, likely lead to a more effective release of DOX inside tumor cells.

Tian *et al.* [179] synthesized an azide-terminated diblock copolymer from oligo(ethylene glycol)methyl ether methacrylate (OEGMA), 2-(diisopropylamino)ethyl methacrylate (DPA), and glycidyl methacrylate (GMA) via consecutive ATRP. The resulting copolymer was then functionalized with DOTA(Gd) and 4-(prop-2-ynyloxy)benzaldehyde and the resulting copolymers were further co-assembled into mixed micellar nanoparticles. The presence of GMA moieties inside the cores enabled encapsulation of tetrakis[4-(2-mercaptoethoxy)phenyl]ethylene (TPE-4SH), and thus the resulting nanoparticles were capable of MR and fluorescence dual imaging. To achieve selective targeting toward tumor tissues and *in situ* drug release, the nanoparticles were surface-conjugated with pH low insertion peptide (pHLIP), which actuated the accumulation of micellar nanoparticles in tumor tissues, confirmed by *in vivo* MR images of tumor-bearing BALB/c nude mice. *In vitro* cytotoxicity study showed that pHLIP also enhanced the release of the loaded cancer drug camptothecin at the tissue site.

Our group and collaborators have recently studied a unibody core-shell (UCS) nanoparticle [180, 181]. These UCS nanoparticles were synthesized using a polymer platform formed by resorcinol and 1,3-phenylenediamine monomers. In the two-step synthesis process, Gd^{3+} was first conjugated to the polymer backbone to form the Gd-core, and then DOX was encapsulated within the shell surrounding the Gd-core. Resorcinol was chosen as one of the components in the core for its stabilizing hydroxyl groups at the physiological pH ranges of interest. 1,3-phenylenediamine was chosen as the shell unit for its capability for pH-controllable release via its amino groups, as demonstrated in **Figure 2** and **Figure 6**. In addition, hydrophobic patches in 1,3-phenylenediamine provide tight packing of DOX molecules, resulting in a superior drug loading efficiency of 97.5%. The design of such UCS-Gd-DOX takes advantage of the acidic pH values of some malignant tumor tissues, ranging around 6.5 [182].

In vitro and *in vivo* studies of UCS-Gd-DOX as an innovative theranostic nanoparticle showed that: (1) DOX in the shell is effectively and selectively released in acidic environments (pH = 5.5) compared to weakly basic (pH = 7.4) physiological environments such as in the blood; (2) the signal-to-noise ratio (SNR) of the "region of interest" (ROI) after injection is increased by 10–30% (n = 3 mice). *In vitro* drug release studies showed that at pH = 8.0, 7.0, 6.0, 5.0, and 4.0, the release of DOX after 2 h was found to be <5%, 10%, 55%, 75%, and 80%, respectively. The increased release of DOX in acidic environments can be attributed to protonation of the polymer backbone. The notable increase in drug release from pH = 7.0 to pH = 6.0 verified the potential of UCS-Gd-DOX for targeted therapy towards malignant tumor tissues. In addition, based on data acquired from *in vitro* T_1-weighted MR images, the r_1 relaxivity of UCS-Gd-DOX at pH = 5.5 was found to be 14.5 mM^{-1} s^{-1}, which was significantly higher than that of UCS-Gd-DOX at pH = 7.4 (0.9 mM^{-1} s^{-1}), overall reflecting the pH-switchable MR contrast capability of UCS-Gd-DOX. We hypothesize this pH-switchability is a result of replacing the water molecules associated to the shell of the nanovehicle with DOX in an acidic condition.

In vivo multiple-slice MR data of 3 mice is shown in **Figure 7**, where T_1-weighted images of NOD/SCID mice with heterotopic, subcutaneous human cervical cancers were acquired and processed with "maximum intensity projection". The contrast of the tumor area increases with time up to 251 min after the injection of UCS-Gd-DOX. This longer contrast enhancement period compared to free Gd-DPTA may be attributed to the longer circulation time of nanoparticles in the blood. The pH-responsive design of the unibody core-shell nanoparticle not only improved the MRI contrast at the tumor site with respect to other tissue/organs, but also successfully suppressed growth of subcutaneous human cervical cancer in mouse xenograft models. As theranostic nanoparticles with Gd-conjugation and DOX-doping can be

synthesized in a straightforward approach, we anticipate further expansive applications of UCS-Gd-DOX in the field of cancer treatment.

3.2.2. Combined therapy

Recent studies also combined chemotherapy with other treatments to achieve a synergistic therapeutic effect. For example, in recent work by Li *et al.* [183], CuS nanoparticles served as the core and were encapsulated by a copolymer shell formed by one-pot emulsifier-free emulsion polymerization of styrene, N-isopropylacrylamide, methacrylic acid, and polymerizable complex $Gd(AA)_3$phen. DOX was then loaded to the copolymer microsphere with a high loading capacity (15.3 wt%). This core-shell nano-platform can be used for photothermal therapy, since the photosensitive CuS cores effectively absorb NIR light and convert NIR light to heat. In addition, the local temperature rise during NIR irradiation shrinks the thermo-sensitive copolymer shell, promoting DOX release at the tumor site. *In vivo* therapeutic study on 4T1 tumor-bearing mice showed that tumor growth was significantly inhibited in the CuS@copolymer/DOX + NIR laser group, compared to other groups (control group, free DOX group, and CuS@copolymer + NIR laser group), which demonstrated the promise of multiple treatment modalities. Gold nanostar (AuNS) can also serve as the core and enable plasmonic photothermal effects [184]. *In vivo* experiments on 4T1 breast tumor-bearing mice showed that AuNS@CP, which was formed by an AuNS core surrounded by a coordination polymers shell composed of the anti-cancer drug gemcitabine-5′-monophosphate (GMP) and Gd(III), significantly suppressed the growth of tumor under laser irradiation (median tumor volume of 138 mm^3 on day 15, n = 5) compared to all 6 control groups (median tumor volume ranged from 447 mm^3 to 1145 mm^3 on day 15).

3.2.3. Other T_1-mode copolymer nanoparticles

In recent years, manganese oxide (MnO_2)—a T_1 contrast agent—has attracted great interest in cancer theranostics because of its additional catalyzing function to decompose endogenous H_2O_2 inside tumors, subsequently contributing to synergistic cancer therapies. For example, Hu *et al.* [185] combined chemotherapy and photodynamic therapy (PDT), which is a recent, minimally-invasive modality that kills cancer cells by the cytotoxic singlet oxygen ($^1O_2$) generated from light-activated photosensitizers. To optimize the efficacy of the combination therapy, they fabricated a multifunctional polymeric nanoparticle system using amphiphilic block copolymer PCLA-PEG-PCLA. MnO_2 and hydrophilic DOX were then loaded in the water phase core, while the photosensitizer chlorin e6 (Ce6) was loaded in the hydrophobic layer. At the tumor location, encapsulated MnO_2 reacted with H_2O_2, a massive tumor metabolite, and generated O_2 for PDT and Mn^{2+} for MRI contrast enhancement. *In vivo* rat experiments showed that the MnO_2-, DOX-, and Ce6-loaded copolymer nanoparticle inhibited tumor growth effectively with an inhibition ratio of 92.35% (calculated by tumor weight), statistically (n =5 for each group) much higher than all 7 control groups. Wang *et al.* [186] used PLGA to load gold nanorods (AuNRs) and DTX to form a PLGA/AuNR/DTX core, then coated it with MnO_2 ultrathin nanofilms. The higher GSH level in the tumor microenvironment caused the degradation of MnO_2 into Mn^{2+}, enabling T_1-MRI as well as controlled release of DTX at the tumor site. The combination of Mn^{2+} and AuNRs enabled T_1-MRI/CT dual imaging, which was confirmed by *in vivo* MRI/CT of mice bearing S-180 sarcoma tumors.

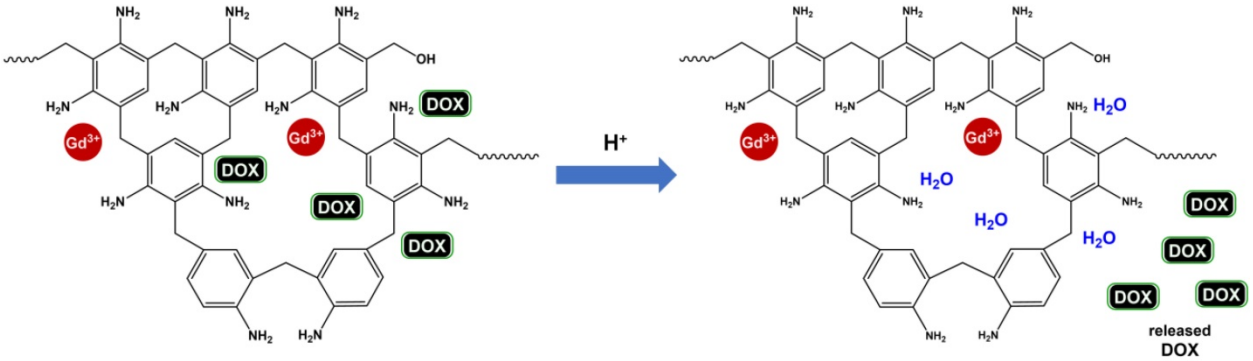

Figure 6. pH-controllable drug delivery and contrast-enhanced MR imaging based on core-shell smart polymer nanoparticles. At low pH, protonation of the amino groups on the shell leads to release of DOX molecules into the bulk solution. Upon release, the empty shell scaffolds take up water molecules, which interact with the inner-layer Gd, enhancing MRI contrast.

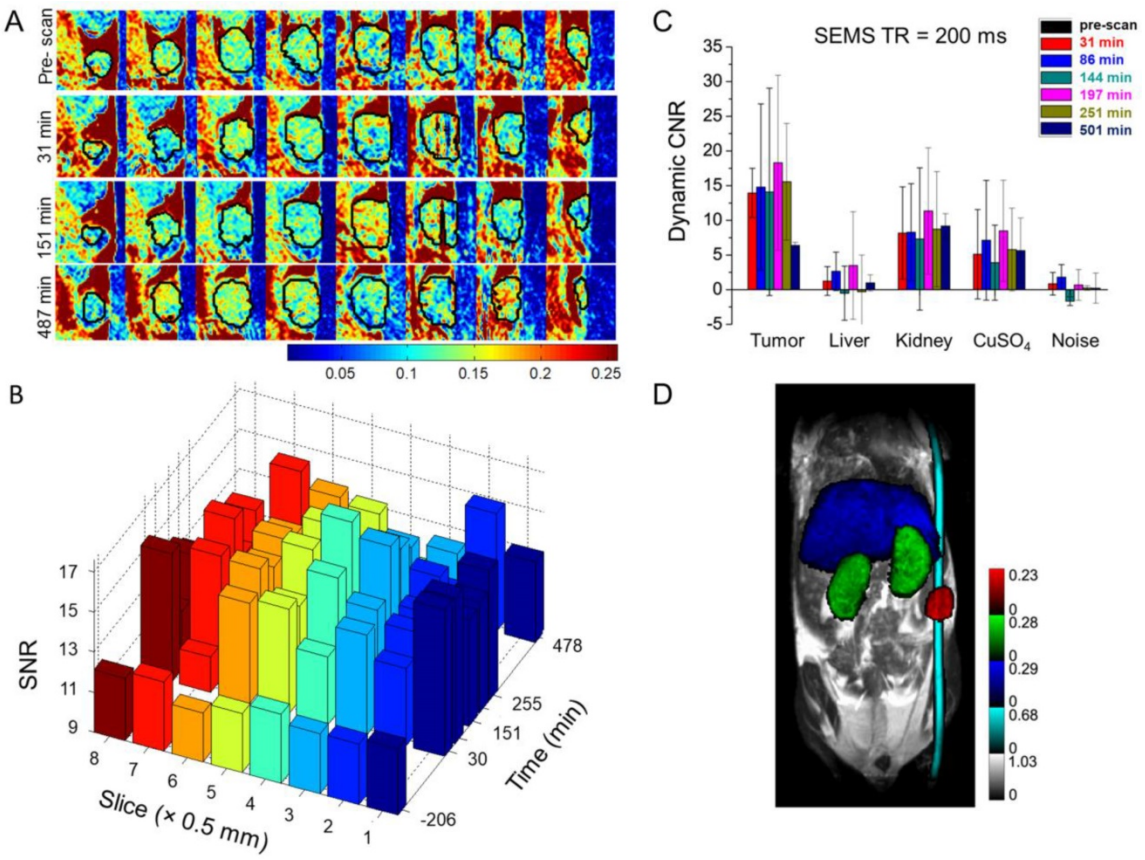

Figure 7. MR analysis of human cervical tumor-bearing mice using UCS-Gd-DOX. **(A)** 2D-slice images of tumor (black circles), where the color bar indicates the MR signal intensity. Only the image pixels with intensity values between ±2 standard deviations (STD) of the ROI signal were kept to avoid image artifacts. **(B)** SNR for each slice in (A) at time points: pre-scan (-206 min), 30 min, 82 min, 151 min, 203 min, 255 min, and 487 min. **(C)** Contrast-to-noise ratio (CNR) of tumor, liver, kidney, $CuSO_4$, and noise area before and after injection. Here CNR % = ($SNR_{postinjection}$ – $SNR_{preinjection}$) / $SNR_{preinjection}$ ×100%. Error bars represent mean ± standard deviation (n = 3 mice). **(D)** T1-weighted MR images acquired by "spin-echo multiple slices" (SEMS) and then processed by "maximum intensity projection". Repetition time (TR) = 200 ms, echo time (TE) = 10 ms, field of view (FOV) = 64×32 mm^2, matrix size = 256×128, slice thickness = 0.5 mm. The ROIs of tumor, liver, kidney, and $CuSO_4$ reference are indicated by red, blue, green, and cyan shades, respectively.

The Liu groups have demonstrated the application of MnO_2 or its complex in core-shell nano-platforms for T_1-weighted MRI and therapy. In one study [187], they designed a nano-platform composed of MnO_2 core and nanoscale coordination polymer shell that is responsive to pH or H_2O_2 concentration. *In vivo* mouse experiments showed that the MR signal intensity in the tumor achieved approximately 2-fold positive enhancement at 12 h post injection. It was further found in the *in vivo* combination therapy that when combined with X-ray irradiation treatment, the nano-platform showed the most effective tumor growth inhibition effect. On Day 14, the tumor volume was approximately 1/6 that of the control group, and 1/4 that of the X-ray radiation alone group. In another study [188], they formed a core-shell structure consisting of Ce6-premodified human serum albumin (HSA-Ce6) core and RGD-premodified HSA (HSA-RGD) shell. Ce6 in the core served as a chelating agent for Mn^{2+} for T_1-weighted MRI and as a photosensitizer for fluorescence imaging, and enabled photodynamic therapy for cancer at the same time. *In vivo* experiments on mice bearing U87MG tumors showed enhancement in both r_1 relaxivity and T_1-weighted MR signal intensity and confirmed the targeting efficiency of RGD. As a result of the combined photodynamic/chemotherapy, the PTX-bound core-shell structure significantly inhibited tumor growth.

In a very recent work [189], Sun *et al.* designed and fabricated a nano-platform for T_1-weighted MR/fluorescence dual-modal imaging and imaging-guided cancer chemotherapy. They first synthesized a PEI-driven self-assembled Gd-/Eu-doped CaF_2 nanocluster (GECN) as the core, loaded the anti-cancer drug cisplatin (CDDP), and then coated the core by PEG-coupled FA. It has been found that inorganic fluorides doped with lanthanides such as Gd and Eu possess excellent fluorescence properties as well as paramagnetic properties [190]. The r_1 rate constant of the nano-platform was measured to be 4.91 mM^{-1} s^{-1}, higher than that of Gd-DTPA (3.34 mM^{-1} s^{-1}). The nano-platform also

displayed better contrast in *in vivo* images of mice bearing HeLa cells compare to Gd-DTPA, resulting from the active FA targeting.

3.3. Heteronuclear copolymer nanoparticles

Similar to fluorinated dendrimers, fluorinated core-shell copolymers have also been used as theranostic agents because of their good biocompatibility and low *in vivo* background signal compared to iron oxide, Gd^{3+}, and Mn oxides. Porsch *et al.* [191] synthesized fluorinated nanoparticles by self-assembly of star-shaped amphiphilic block copolymers. The hydrophilic segment of the copolymer was formed by the polymerization of monomers OEGMA and trifluoroethyl methacrylate (TFEMA) via ATRP. TFEMA was chosen for its chemically equivalent fluorine atoms that are able to produce optimal MRI signal, and OEGMA was chosen for its hydrophilic and highly dynamic structure, which was hypothesized by the authors to facilitate the mobility of the fluorine atoms of TFEMA. The authors studied five star-shaped copolymers with different numbers of arms (4 or 16 arms) and different molecular weights ranging from 10k to 52k, and noticed that larger hydrophobic cores increased the loading capacity of DOX while larger hydrophilic shells decreased it. *In vitro* studies showed that the designed nanoparticles can be taken up by breast cancer cells and deliver DOX into the cell nuclei with controllable drug release kinetics.

Perfluorooctyl bromide (PFOB) has attracted great attention in more recent work on fluorinated copolymer contrast agents, since it is approved by the FDA due to its safety. For example, Boissenot *et al.* [192] encapsulated PTX in core-shell nanocapsules made of a PFOB core and PLGA-PEG shell. ^{19}F MRI confirmed the passive accumulation of the core-shell nanoparticles to the tumor site, which led to a statistically (n = 9) significant 2-fold reduction in tumor growth of the mice at 10–12 days after CT-26 cells induction compared to the negative control or the generic PTX groups. Quang *et al.* [193] formed nanoparticles consisting of a PFOB core and a shell of PLGA followed by a coat of polystyrene sulfonate (PSS), which can facilitate entry of the nanoparticles into cells via caveolae-mediated endocytosis. *In vivo* study in normal BALB/c mice and immune-compromised NOD/SCID mice showed that one week after transplantation of human cells, 40% of the ^{19}F MRI signal was lost in normal mice, while only 10% was lost in immune-compromised mice, proving the potential use of this PSS-coated core-shell nanoparticle as a prognostic indicator for immune rejection in stem cell therapy.

4. Major challenges and safety aspects for clinical uses

Specific theranostic approaches for drug delivery could be very promising directions for detecting and eliminating cancer lesions at early stages, providing new hope to cancer patients worldwide. Unfortunately, this area of treatment still suffers from several safety issues and challenges. Firstly, the use of a high dose of Gd(III) is toxic to the kidney, thus the FDA does not approve administering Gd(III)-based drugs to patients with any serious renal problems. Although the alternative SPIO is a safer and biodegradable material, T_2-weighted MR imaging shows a negative contrast in comparison to T_1-weighted positive contrast, making it less efficient for differentiating tumor tissues from healthy tissues. Pharmacokinetic considerations and biodistribution studies of specific nanoconstructs are very important for successful *in vivo* applications and clinical translation [194]. Major concerns for the use of either the dendrimer or the core-shell copolymer are material toxicity, rapid clearance from the body, imperfect biodistribution, and incomplete biodegradability [1]. However, PEGylation and other surface modifications could decrease the toxicity of the dendrimer to healthy tissues [25]. A potential solution for the dendrimer nanovehicle would be to use a peptide-like dendrimer having similar properties to those of protein and thus be biodegradable. Recently, lysine polypeptides or amino acid-based dendrimers have been developed [60] as biodegradable alternatives for delivery nanovehicles, and show future promise for clinical use [195]. A comprehensive discussion on the biodegradability of different kinds of dendrimers can be found in a recent review by Leiro *et al.* [196]. Core-shell copolymers could also be modified using polyesters such as PLGA, PLA, or poly(glycolide) as the polymer backbone to enhance biocompatibility and biodegradability [197–199].

Some of the approaches discussed in this review rely on pH-controlled delivery that is not very specific towards early tumors, as the pH values of early tumors are generally not very different from those of normal tissues. Therefore, more investigations are required in this line for controlled drug delivery. Similarly, passive targeting has its limitations [200]. Unlike passive targeting, active targeting relies on cell specific recognition via target specific ligand binding and internalization happens through receptor-mediated endocytosis. Hence, nanoparticles are potent to be accumulated in tumor site in a higher concentration via active targeting, compared to passive targeting. Therefore, as discussed, future

advancements should aim to upgrade all the theranostic structures to include active targeting moieties to specifically target cancer cells and minimize adverse side effects to healthy cells. Further clinical trials and experiments are required to optimize the safety, viability, and applicability of different nanovehicles before they could be used for clinical purposes.

5. Conclusion

We have discussed the current status of research on MR-guided theranostic uses of polymer-like nanostructures such as dendrimer and copolymer core-shell-based nanoparticles. Polymer-like structures provide a means to target the tumor site and deliver the required amount of drug there while minimizing adverse side effects to surrounding healthy tissues. Several types of cancers such as pancreatic cancer cannot be treated by conventional chemotherapy, because the medicine cannot reach the tumor site due to the resistance offered by the surrounding stroma. However, ATRA-conjugated dendrimer-coated SPIO have the potential to overcome this resistance and deliver medicine to the tumor site [38] as described in section 2.1.1. Moreover, this type of theranostic could reduce the need for surgery, or increase the efficiency of surgical removal of the tumor to make the treatment as noninvasive as possible. However, the safety issues have not yet been fully resolved and FDA approval is still pending for the use of these types of nanovehicles for cancer therapy. This platform is still very young but developing rapidly. Regardless of the many hurdles and difficulties, the uses of dendrimer and copolymer core-shell nanovehicles provide a very promising direction for future nanomedicine and cancer therapy.

Abbreviations

Ad: adamantane; AMF: alternating magnetic field; ATRA: all-*trans* retinoic acid; ATRP: atom transfer radical polymerization; BCNU: 1,3-bis(2-chloroethyl)-1-nitrosourea; CD: cyclodextrin; CDF: 3,4-difluorobenzylidene-curcumin; Ce6: chlorin e6; DDACMM: [7-(didodecylamino)coumarin-4-yl] methyl methacrylate; DOX: doxorubicin; DTX: docetaxel; EPR: enhanced permeability and retention effect; FA: folic acid; G: generation; Gd: gadolinium; GSH: glutathione tripeptide; HIFU: high-intensity focused ultrasound; LHRH: luteinizing hormone-releasing hormone; mcDNA: minicircle DNA; mPEG: methoxy poly(ethylene glycol); mPEG-CHO: methoxypoly(ethylene glycol) benzaldehyde; MPS: mononuclear phagocyte system; MRI: magnetic resonance imaging; MT: magnetic targeting; NIR: near-infrared; OEGMA: oligo (ethylene glycol) methyl ether methacrylate; PAMAM: polyamidoamine; PBLA: poly(benzyl L-aspartate); PCL: poly ε-caprolactone; PDMAEMA: poly(2-dimethylaminoethyl methacrylate); pDNA: plasmid DNA; PEG: polyethylene glycol; PEI: polyethylenimine; PFH: perfluorohexane; poly I:C : polyinosinic:polycytidylic acid; PLA: poly(D,L lactide); PLGA: poly(D,L-lactic-co-glycolic acid); PNIPAM: poly(N-isopropylacrylamide); PPEGMA: poly(poly(ethylene glycol) methyl ether methacrylate); PPI: poly(propyleneimine); PPSu: poly(propylene succinate); PSC: pancreatic stellate cells; PS-b-PAA: poly(styrene)-b-poly(acrylic acid); PTX: paclitaxel; ROI: region of interest; scAb: stem cell antibody; siRNA: short interfering RNA; SNR: signal-to-noise ratio; SNP: supramolecular nanoparticle; SPECT: single-photon emission computed tomography; SPIO: superparamagnetic iron oxide; UCS: unibody core-shell.

Acknowledgments

This work was supported by the National Science Foundation (CHE-1112574 and CHE-1416598), University of California Cancer Research Award (CRR-13-201412), Hirshberg Foundation for Pancreatic Cancer Research, and Taiwan Ministry of Science and Technology (NSC 100-2113-M-002-008, NSC 101-2113-M-002-018, and MOST 103-2923-M-002-006). The authors thank Ms. Sheba Plamthottam for graphics assistance.

Competing Interests

The authors have declared that no competing interest exists.

References

1. Janib SM, Moses AS, MacKay JA. Imaging and drug delivery using theranostic nanoparticles. Adv Drug Deliv Rev. 2010; 62: 1052–1063
2. Sunderland CJ, Steiert M, Talmadge JE, et al. Targeted nanoparticles for detecting and treating cancer. Drug Dev Res. 2006; 67: 70–93
3. Kelkar SS, Reineke TM. Theranostics: Combining imaging and therapy. Bioconjug Chem. 2011; 22: 1879–1903
4. Key J, Leary JF. Nanoparticles for multimodal in vivo imaging in nanomedicine. Int J Nanomedicine. 2014; 9: 711–726
5. Huang G, Chen H, Dong Y, et al. Superparamagnetic iron oxide nanoparticles: Amplifying ros stress to improve anticancer drug efficacy. Theranostics. 2013; 3: 116–126
6. Yen SK, Padmanabhan P, Selvan ST. Multifunctional iron oxide nanoparticles for diagnostics, therapy and macromolecule delivery. Theranostics. 2013; 3: 986–1003
7. Kotb S, Detappe A, Lux F, et al. Gadolinium-based nanoparticles and radiation therapy for multiple brain melanoma metastases: Proof of concept before phase I trial. Theranostics. 2016; 6: 418–427
8. Merbach A, Helm L, Tóth E. The chemistry of contrast agents in medical magnetic resonance imaging. 2nd ed. Chichester, UK: Wiley; 2013
9. Li M, Kim HS, Tian L, et al. Comparison of two ultrasmall superparamagnetic iron oxides on cyto-toxicity and MR imaging of tumors. Theranostics. 2012; 2: 76–85
10. Ho DN, Kohler N, Sigdel A, et al. Penetration of endothelial cell coated multicellular tumor spheroids by iron oxide nanoparticles. Theranostics. 2012; 2: 66–75
11. Li L, Jiang W, Luo K, et al. Superparamagnetic iron oxide nanoparticles as MRI contrast agents for non-invasive stem cell labeling and tracking. Theranostics. 2013; 3: 595–615

12. Li Z, Hsu C-H, Dimitrov N, et al. Sensitive imaging of magnetic nanoparticles for cancer detection by active feedback MR. Magn Reson Med. 2015; 74: 33–41
13. Wang C, Li Z, Lin Y-Y. Optimizing magnetic nanoparticle hyperthermia effect in MR nanomedicine. Chin J Magn Reson. 2015; 32(2): 248–260.
14. Lin F-C, Hsu C-H, Lin Y-Y. Nano-therapeutic cancer immunotherapy using hyperthermia-induced heat shock proteins: insights from mathematical modeling. Int J Nanomedicine. 2018; 13: 1–11
15. Wu W, Luo L, Wang Y, et al. Endogenous pH-responsive nanoparticles with programmable size changes for targeted tumor therapy and imaging applications. Theranostics. 2018; 8: 3038
16. Peer D, Karp JM, Hong S, et al. Nanocarriers as an emerging platform for cancer therapy. Nat Nanotechnol. 2007; 2: 751–760
17. Wang Z, Niu G, Chen X. Polymeric materials for theranostic applications. Pharm Res. 2014; 31: 1358–1376
18. Kesharwani P, Jain K, Jain NK. Dendrimer as nanocarrier for drug delivery. Prog Polym Sci. 2014; 39: 268-307
19. Zhao Y, Liu S, Li Y, et al. Synthesis and grafting of folate–PEG–PAMAM conjugates onto quantum dots for selective targeting of folate-receptor-positive tumor cells. J Colloid Interface Sci. 2010; 350: 44–50
20. Tomalia DA, Reyna LA, Svenson S. Dendrimers as multi-purpose nanodevices for oncology drug delivery and diagnostic imaging. Biochem Soc Trans. 2007; 35: 61–67
21. Cheng Y, Zhao L, Li Y, et al. Design of biocompatible dendrimers for cancer diagnosis and therapy: current status and future perspectives. Chem Soc Rev. 2011; 40: 2673–2703
22. Ma Y, Mou Q, Wang D, et al. Dendritic polymers for theranostics. Theranostics. 2016; 6: 930–947
23. Svenson S, Tomalia DA. Dendrimers in biomedical applications—reflections on the field. Adv Drug Deliv Rev. 2012; 64: 102–115
24. Tomalia DA, Baker H, Dewald J, et al. A new class of polymers: Starburst-dendritic macromolecules. Polym J. 1985; 17: 117–132
25. Lo S-T, Kumar A, Hsieh J-T, et al. Dendrimer nanoscaffolds for potential theranostics of prostate cancer with a focus on radiochemistry. Mol Pharm. 2013; 10: 793–812
26. Fréchet JMJ, Tomalia DA. Dendrimers and other dendritic polymers. Chichester, UK: Wiley; 2001
27. Colombo M, Carregal-Romero S, Casula MF, et al. Biological applications of magnetic nanoparticles. Chem Soc Rev. 2012; 41: 4306–4334
28. Sun W, Mignani S, Shen M, et al. Dendrimer-based magnetic iron oxide nanoparticles: their synthesis and biomedical applications. Drug Discov Today. 2016; 21: 1873–1885
29. Scherer F, Anton M, Schillinger U, et al. Magnetofection: enhancing and targeting gene delivery by magnetic force in vitro and in vivo. Gene Ther. 2002; 9: 102–109
30. Liu W-M, Xue Y-N, Peng N, et al. Dendrimer modified magnetic iron oxide nanoparticle/DNA/PEI ternary magnetoplexes: a novel strategy for magnetofection. J Mater Chem. 2011; 21: 13306-13315
31. Matsumura Y, Maeda H. A new concept for macromolecular therapeutics in cancer chemotherapy: mechanism of tumoritropic accumulation of proteins and the antitumor agent smancs. Cancer Res. 1986; 46: 6387–6392
32. Duncan R. Tumour targeting by enhanced permeability and retention (EPR) effect. Ann Oncol. 1998; 9: 39
33. Singal P, Li T, Kumar D, et al. Adriamycin-induced heart failure: mechanisms and modulation. Mol Cell Biochem. 2000; 207: 77–86
34. Khodadust R, Unsoy G, Gunduz U. Development of poly (I:C) modified doxorubicin loaded magnetic dendrimer nanoparticles for targeted combination therapy. Biomed Pharmacother. 2014; 68: 979–987
35. Rouhollah K, Pelin M, Serap Y, et al. Doxorubicin loading, release, and stability of polyamidoamine dendrimer-coated magnetic nanoparticles. J Pharm Sci. 2013; 102: 1825–1835
36. Weber A, Kirejczyk Z, Besch R, et al. Proapoptotic signalling through Toll-like receptor-3 involves TRIF-dependent activation of caspase-8 and is under the control of inhibitor of apoptosis proteins in melanoma cells. Cell Death Differ. 2010; 17: 942–951
37. Salvador A, Igartua M, Hernández RM, et al. Combination of immune stimulating adjuvants with poly(lactide-co-glycolide) microspheres enhances the immune response of vaccines. Vaccine. 2012; 30: 589–596
38. Yalçın S, Erkan M, Ünsoy G, et al. Effect of gemcitabine and retinoic acid loaded PAMAM dendrimer-coated magnetic nanoparticles on pancreatic cancer and stellate cell lines. Biomed Pharmacother. 2014; 68: 737–743
39. Apte M V, Haber PS, Applegate TL, et al. Periacinar stellate shaped cells in rat pancreas: identification, isolation, and culture. Gut. 1998; 43: 128–133
40. Michael A, Hill M, Maraveyas A, et al. 13-cis-Retinoic acid in combination with gemcitabine in the treatment of locally advanced and metastatic pancreatic cancer—Report of a pilot phase II study. Clin Oncol. 2007; 19: 150–153
41. Weitman SD, Lark RH, Coney LR, et al. Distribution of the folate receptor GP38 in normal and malignant cell lines and tissues. Cancer Res. 1992; 52: 3396–3401
42. Shi X, Wang SH, Swanson SD, et al. Dendrimer-functionalized shell-crosslinked iron oxide nanoparticles for in-vivo magnetic resonance imaging of tumors. Adv Mater. 2008; 20: 1671–1678
43. Chang Y, Liu N, Chen L, et al. Synthesis and characterization of DOX-conjugated dendrimer-modified magnetic iron oxide conjugates for magnetic resonance imaging, targeting, and drug delivery. J Mater Chem. 2012; 22: 9594–9601
44. Chang Y, Meng X, Zhao Y, et al. Novel water-soluble and pH-responsive anticancer drug nanocarriers: Doxorubicin–PAMAM dendrimer conjugates attached to superparamagnetic iron oxide nanoparticles (IONPs). J Colloid Interface Sci. 2011; 363: 403–409
45. Kesharwani P, Banerjee S, Padhye S, et al. Parenterally administrable nano-micelles of 3,4-difluorobenzylidene curcumin for treating pancreatic cancer. Colloids Surf B. 2015; 132: 138–145
46. Padhye S, Banerjee S, Chavan D, et al. Fluorocurcumins as cyclooxygenase-2 inhibitor: molecular docking, pharmacokinetics and tissue distribution in mice. Pharm Res. 2009; 26: 2438–2445
47. Luong D, Kesharwani P, Killinger BA, et al. Solubility enhancement and targeted delivery of a potent anticancer flavonoid analogue to cancer cells using ligand decorated dendrimer nano-architectures. J Colloid Interface Sci. 2016; 484: 33–43
48. Luong D, Sau S, Kesharwani P, et al. Polyvalent folate-dendrimer-coated iron oxide theranostic nanoparticles for simultaneous magnetic resonance imaging and precise cancer cell targeting. Biomacromolecules. 2017; 18: 1197–1209
49. Kerbel RS, Kamen BA. The anti-angiogenic basis of metronomic chemotherapy. Nat Rev Cancer. 2004; 4: 423–436
50. Lin X, Deng L, Xu Y, et al. Thermosensitive in situ hydrogel of paclitaxel conjugated poly(ε-caprolactone)-poly(ethylene glycol)-poly(ε-caprolactone). Soft Matter. 2012; 8: 3470-3477
51. Chang Y, Li Y, Meng X, et al. Dendrimer functionalized water soluble magnetic iron oxide conjugates as dual imaging probe for tumor targeting and drug delivery. Polym Chem. 2013; 4: 789–794
52. Dayyani N, Khoee S, Ramazani A. Design and synthesis of pH-sensitive polyamino-ester magneto-dendrimers: Surface functional groups effect on viability of human prostate carcinoma cell lines DU145. Eur J Med Chem. 2015; 98: 190–202
53. He X, Wu X, Cai X, et al. Functionalization of magnetic nanoparticles with dendritic–linear–brush-like triblock copolymers and their drug release properties. Langmuir. 2012; 28: 11929–11938
54. Wu X, He X, Zhong L, et al. Water-soluble dendritic-linear triblock copolymer-modified magnetic nanoparticles: preparation, characterization and drug release properties. J Mater Chem. 2011; 21: 13611-13620
55. Park J, Yu MK, Jeong YY, et al. Antibiofouling amphiphilic polymer-coated superparamagnetic iron oxide nanoparticles: synthesis, characterization, and use in cancer imaging in vivo. J Mater Chem. 2009; 19: 6412-6417
56. Lattuada M, Hatton TA. Functionalization of monodisperse magnetic nanoparticles. Langmuir. 2007; 23: 2158–2168
57. Chandra S, Dietrich S, Lang H, et al. Dendrimer–doxorubicin conjugate for enhanced therapeutic effects for cancer. J Mater Chem. 2011; 21: 5729-5737
58. Wei H, Cheng S-X, Zhang X-Z, et al. Thermo-sensitive polymeric micelles based on poly(N-isopropylacrylamide) as drug carriers. Prog Polym Sci. 2009; 34: 893–910
59. Khoee S, Hemati K. Synthesis of magnetite/polyamino-ester dendrimer based on PCL/PEG amphiphilic copolymers via convergent approach for targeted diagnosis and therapy. Polym. (United Kingdom). 2013; 54: 5574–5585
60. Nigam S, Bahadur D. Dendrimer-conjugated iron oxide nanoparticles as stimuli-responsive drug carriers for thermally-activated chemotherapy of cancer. Colloids Surf B. 2017; 155: 182–192
61. Liu G, Swierczewska M, Lee S, et al. Functional nanoparticles for molecular imaging guided gene delivery. Nano Today. 2010; 5: 524–539
62. Mintzer MA, Simanek EE. Nonviral vectors for gene delivery. Chem Rev. 2009; 109: 259–302
63. Wang K, Wang K, Shen B, et al. MR reporter gene imaging of endostatin expression and therapy. Mol Imaging Biol. 2010; 12: 520–529
64. Xiao S, Castro R, Rodrigues J, et al. PAMAM dendrimer/pDNA functionalized-magnetic iron oxide nanoparticles for gene delivery. J Biomed Nanotechnol. 2015; 11: 1370–1384
65. Ch'ng JL, Mulligan RC, Schimmel P, et al. Antisense RNA complementary to 3′ coding and noncoding sequences of creatine kinase is a potent inhibitor of translation in vivo. Proc Natl Acad Sci U. S. A. 1989; 86: 10006–10010
66. Denhardt DT. Mechanism of action of antisense RNA. Sometime inhibition of transcription, processing, transport, or translationa. Ann N. Y. Acad Sci. 1992; 660: 70–76
67. Kim SH, Mok H, Jeong JH, et al. Comparative evaluation of target-specific GFP gene silencing efficiencies for antisense ODN, synthetic siRNA, and siRNA plasmid complexed with PEI−PEG−FOL conjugate. Bioconjug Chem. 2006; 17: 241–244
68. Pan B, Cui D, Sheng Y, et al. Dendrimer-modified magnetic nanoparticles enhance efficiency of gene delivery system. Cancer Res. 2007; 67: 8156–8163
69. Zhang Z, Cao X, Zhao X, et al. Controlled delivery of antisense oligodeoxynucleotide from cationically modified phosphorylcholine polymer films. Biomacromolecules. 2006; 7: 784–791
70. Dykxhoorn DM, Lieberman J. The silent revolution: RNA interference as basic biology, research tool, and therapeutic. Annu Rev Med. 2005; 56: 401–423
71. Uprichard SL. The therapeutic potential of RNA interference. FEBS Lett. 2005; 579: 5996–6007
72. Gary DJ, Puri N, Won Y-Y. Polymer-based siRNA delivery: Perspectives on the fundamental and phenomenological distinctions from polymer-based DNA delivery. J Control Release. 2007; 121: 64–73

73. Ikeda Y, Taira K. Ligand-targeted delivery of therapeutic siRNA. Pharm Res. 2006; 23: 1631–1640
74. Taratula O, Garbuzenko O, Savla R, et al. Multifunctional nanomedicine platform for cancer specific delivery of siRNA by superparamagnetic iron oxide nanoparticles-dendrimer complexes. Curr Drug Deliv. 2011; 8: 59–69
75. Dharap SS, Minko T. Targeted proapoptotic LHRH-BH3 peptide. Pharm Res. 2003; 20: 889–896
76. Dharap SS, Wang Y, Chandna P, et al. Tumor-specific targeting of an anticancer drug delivery system by LHRH peptide. Proc Natl Acad Sci U. S. A. 2005; 102: 12962–12967
77. Unsoy G, Yalcin S, Khodadust R, et al. PAMAM dedrimer coated MNPs for siRNA delivery and gene silencing. J Cancer Stud Ther. 2014; 1: 1–5
78. Agrawal A, Min DH, Singh N, et al. Functional delivery of siRNA in mice using dendriworms. ACS Nano. 2009; 3: 2495–2504
79. Kesharwani P, Banerjee S, Gupta U, et al. PAMAM dendrimers as promising nanocarriers for RNAi therapeutics. Mater Today. 2015; 18: 565–572
80. Li J, Liang H, Liu J, et al. Poly (amidoamine) (PAMAM) dendrimer mediated delivery of drug and pDNA/siRNA for cancer therapy. Int J Pharm. 2018; 546: 215–225
81. Dobson J. Gene therapy progress and prospects: magnetic nanoparticle-based gene delivery. Gene Ther. 2006; 13: 283–287
82. Tschulik K, Compton RG. Nanoparticle impacts reveal magnetic field induced agglomeration and reduced dissolution rates. Phys Chem Chem Phys. 2014; 16: 13909–13913
83. Xie J, Chen K, Lee H, et al. Ultra-small c(RGDyK)-coated Fe_3O_4 nanoparticles and their specific targeting to integrin α. J Am Chem Soc. 2008; 130: 7542–7543
84. Yang J, Luo Y, Xu Y, et al. Conjugation of iron oxide nanoparticles with RGD-modified dendrimers for targeted tumor MR imaging. ACS Appl Mater Interfaces. 2015; 7: 5420–5428
85. Bumb A, Brechbiel MW, Choyke PL, et al. Synthesis and characterization of ultra-small superparamagnetic iron oxide nanoparticles thinly coated with silica. Nanotechnology. 2008; 19: 335601
86. Cai W, Shin DW, Chen K, et al. Peptide-labeled near-infrared quantum dots for imaging tumor vasculature in living subjects. Nano Lett. 2006; 6: 669–676
87. Li Z-B, Cai W, Cao Q, et al. 64 Cu-labeled tetrameric and octameric RGD peptides for small-animal PET of tumor αvβ3 integrin expression. J Nucl Med. 2007; 48: 1162–1171
88. Zhu J, Xiong Z, Shen M, et al. Encapsulation of doxorubicin within multifunctional gadolinium-loaded dendrimer nanocomplexes for targeted theranostics of cancer cells. RSC Adv. 2015; 5: 30286–30296
89. Percec V, Wilson DA, Leowanawat P, et al. Self-assembly of Janus dendrimers into uniform dendrimersomes and other complex architectures. Science. 2010; 328: 1009–1014
90. Filippi M, Catanzaro V, Patrucco D, et al. First in vivo MRI study on theranostic dendrimersomes. J Control Release. 2017; 248: 45–52
91. Kamaly N, Miller AD. Paramagnetic liposome nanoparticles for cellular and tumour imaging. Int J Mol Sci. 2010; 11: 1759–1776
92. Wang Q, Li J, An S, et al. Magnetic resonance-guided regional gene delivery strategy using a tumor stroma-permeable nanocarrier for pancreatic cancer. Int J Nanomedicine. 2015; 10: 4479–4490
93. Tilcock C, Unger E, Cullis P, et al. Liposomal Gd-DTPA: Preparation and characterization of relaxivity. Radiology. 1989; 171: 77–80
94. Cheng Z, Thorek DLJ, Tsourkas A. Gadolinium-conjugated dendrimer nanoclusters as a tumor-targeted T1 magnetic resonance imaging contrast agent. Angew Chem Int Ed Engl. 2010; 49: 346–350
95. Cheng Z, Thorek DLJ, Tsourkas A. Porous polymersomes with encapsulated Gd-labeled dendrimers as highly efficient MRI contrast agents. Adv Funct Mater. 2009; 19: 3753–3759
96. Chen K-J, Wolahan SM, Wang H, et al. A small MRI contrast agent library of gadolinium(III)-encapsulated supramolecular nanoparticles for improved relaxivity and sensitivity. Biomaterials. 2011; 32: 2160–2165
97. Wiener C, Fauci AS, Braunwald E, et al. Harrison's principles of internal medicine, self-assessment and board review. 18 ed. New york: McGraw-Hill Education; 2008
98. Wang H, Chen K-J, Wang S, et al. A small library of DNA-encapsulated supramolecular nanoparticles for targeted gene delivery. Chem Commun. 2010; 46: 1851-1853
99. Wang H, Liu K, Chen K-J, et al. A rapid pathway toward a superb gene delivery system: Programming structural and functional diversity into a supramolecular nanoparticle library. ACS Nano. 2010; 4: 6235–6243
100. Wang S, Chen K-J, Wu T-H, et al. Photothermal effects of supramolecularly assembled gold nanoparticles for the targeted treatment of cancer cells. Angew Chem Int Ed Engl. 2010; 49: 3777–3781
101. Lee J-H, Chen K-J, Noh S-H, et al. On-demand drug release system for in vivo cancer treatment through self-assembled magnetic nanoparticles. Angew Chem Int Ed Engl. 2013; 125: 4480–4484
102. Tan M, Ye Z, Lindner D, et al. Synthesis and evaluation of a targeted nanoglobular dual-modal imaging agent for MR imaging and image-guided surgery of prostate cancer. Pharm Res. 2014; 31: 1469–1476
103. Pilch J, Brown DM, Komatsu M, et al. Peptides selected for binding to clotted plasma accumulate in tumor stroma and wounds. Proc Natl Acad Sci U. S. A. 2006; 103: 2800–2804
104. Tan M, Burden-Gulley SM, Li W, et al. MR molecular imaging of prostate cancer with a peptide-targeted contrast agent in a mouse orthotopic prostate cancer model. Pharm Res. 2012; 29: 953–960
105. Sonmez H, Suer S, Karaarslan I, et al. Tissue fibronectin levels of human prostatic cancer, as a tumor marker. Cancer Biochem Biophys. 1995; 15: 107–110
106. Tan M, Ye Z, Jeong EK, et al. Synthesis and evaluation of nanoglobular macrocyclic Mn(II) chelate conjugates as non-gadolinium(III) MRI contrast agents. Bioconjug Chem. 2011; 22: 931–937
107. Su H, Wu C, Zhu J, et al. Rigid Mn(II) chelate as efficient MRI contrast agent for vascular imaging. Dalt Trans. 2012; 41: 14480–14483
108. De Sá A, Bonnet CS, Geraldes CFGC, et al. Thermodynamic stability and relaxation studies of small, triaza-macrocyclic Mn(ii) chelates. Dalt Trans. 2013; 42: 4522–4532
109. Bhyrappa P, Young JK, Moore JS, et al. Dendrimer-metalloporphyrins: Synthesis and catalysis. J Am Chem Soc. 1996; 118: 5708–5711
110. Ding L, Lyu Z, Dhumal D, et al. Dendrimer-based magnetic resonance imaging for brain cancer. Sci CHINA Mater. 2018; https://doi.org/10.1007/s40843-018-9323-6
111. Pan D, Schmieder A, Wickline S, et al. Manganese-based MRI contrast agents: past, present and future. Tetrahedron. 2011; 67: 8431–8444
112. Bertin A, Gallani J. Development of a dendritic manganese-enhanced magnetic resonance imaging (MEMRI) contrast agent: Synthesis, toxicity (in vitro) and relaxivity (in vitro, in vivo) studies. Bioconjugate Chem. 2009; 20: 760–767
113. Zhu J, Gale EM, Atanasova I, et al. Hexameric Mn II dendrimer as MRI contrast agent. Chem Eur J. 2014; 20: 14507–14513
114. Keshavarz A, Hajbabaei S, Sojoodi J, et al. Mn^{2+} negatively charged pegylated dendrimer G2-tryptophan: Novel nano magnetic resonance imaging agent. Adv Appl Physiol. 2017; 2: 1–9
115. Tan M, Wu X, Jeong E-K, et al. An effective targeted nanoglobular manganese(II) chelate conjugate for magnetic resonance molecular imaging of tumor extracellular matrix. Mol Pharmacol. 2010; 7: 936–943
116. Menjoge AR, Kannan RM, Tomalia DA. Dendrimer-based drug and imaging conjugates: design considerations for nanomedical applications. Drug Discov Today. 2010; 15: 171–185
117. Jennings L, Long N. Two is better than one'—probes for dual-modality molecular imaging. Chem Commun. 2009; 24: 3511–3524
118. Yang H, Qin C, Yu C, et al. RGD-conjugated nanoscale coordination polymers for targeted T_1- and T_2-weighted magnetic resonance imaging of tumors in vivo. Adv Funct Mater. 2014; 24: 1738–1747
119. Haribabu V, Farook AS, Goswami N, et al. Optimized Mn-doped iron oxide nanoparticles entrapped in dendrimer for dual contrasting role in MRI. J Biomed Mater Res B. 2016; 104: 817–824
120. Pradhan P, Giri J, Banerjee R, et al. Preparation and characterization of manganese ferrite-based magnetic liposomes for hyperthermia treatment of cancer. J Magn Magn Mater. 2007; 311: 208–215
121. Tang Z., Sorensen C., Klabunde K, et al. Preparation of manganese ferrite fine particles from aqueous solution. J Colloid Interface Sci. 1991; 146: 38–52
122. Wen S, Li K, Cai H, et al. Multifunctional dendrimer-entrapped gold nanoparticles for dual mode CT/MR imaging applications. Biomaterials. 2013; 34: 1570–1580
123. Chen Q, Li K, Wen S, et al. Targeted CT/MR dual mode imaging of tumors using multifunctional dendrimer-entrapped gold nanoparticles. Biomaterials. 2013; 34: 5200–5209
124. Li K, Wen S, Larson AC, et al. Multifunctional dendrimer-based nanoparticles for in vivo MR/CT dual-modal molecular imaging of breast cancer. Int J Nanomedicine. 2013; 8: 2589–2600
125. Chen Q, Wang H, Liu H, et al. Multifunctional dendrimer-entrapped gold nanoparticles modified with RGD peptide for targeted computed tomography/magnetic resonance dual-modal imaging of tumors. Anal Chem. 2015; 87: 3949–3956
126. Cai H, Li K, Li J, et al. Dendrimer-assisted formation of Fe_3O_4/Au nanocomposite particles for targeted dual mode CT/MR imaging of tumors. Small 2015; 11: 4584–4593
127. Luo Y, Zhao L, Li X, et al. The design of a multifunctional dendrimer-based nanoplatform for targeted dual mode SPECT/MR imaging of tumors. J Mater Chem B. 2016; 4: 7220–7225
128. Landmark KJ, Dimaggio S, Ward J, et al. Synthesis, characterization, and in vitro testing of superparamagnetic iron oxide nanoparticles targeted using folic acid-conjugated dendrimers. ACS Nano. 2008; 2: 773–783
129. Talanov VS, Regino CAS, Kobayashi H, et al. Dendrimer-based nanoprobe for dual modality magnetic resonance and fluorescence imaging. Nano Lett. 2006; 6: 1459–1463
130. Chen J, Sun Y, Chen Q, et al. Multifunctional gold nanocomposites designed for targeted CT/MR/optical trimodal imaging of human non-small cell lung cancer cells. Nanoscale. 2016; 8: 13568–13573
131. Percec V, Glodde M, Johansson G, et al. Transformation of a spherical supramolecular dendrimer into a pyramidal columnar supramolecular dendrimer mediated by the fluorophobic effect. Angew Chem Int Ed Engl. 2003; 115: 4474–4478
132. Percec V, Johansson G, Ungar G, et al. Fluorophobic effect induces the self-assembly of semifluorinated tapered monodendrons containing crown ethers into supramolecular columnar dendrimers which exhibit a homeotropic hexagonal columnar liquid crystalline phase. J Am Chem Soc. 1996; 118: 9855–9866

133. Liu X, Yuan Y, Bo S, et al. Monitoring fluorinated dendrimer-based self-assembled drug-delivery systems with ^{19}F magnetic resonance. European J Org Chem. 2017; 2017: 4461–4468
134. Criscione JM, Le BL, Stern E, et al. Self-assembly of pH-responsive fluorinated dendrimer-based particulates for drug delivery and noninvasive imaging. Biomaterials. 2009; 30: 3946–3955
135. Martin OM, Yu L, Mecozzi S. Solution self-assembly and solid state properties of fluorinated amphiphilic calix[4]arenes. Chem Commun. 2005; 0: 4964–4966
136. Kimura A, Narazaki M, Kanazawa Y, et al. 19F Magnetic resonance imaging of perfluorooctanoic acid encapsulated in liposome for biodistribution measurement. Magn Reson Imaging. 2004; 22: 855–860
137. Pykett IL, Rosen BR. Nuclear magnetic resonance: in vivo proton chemical shift imaging. Work in progress. Radiology. 1983; 149: 197–201
138. Li Y, Xiao K, Luo J, et al. A novel size-tunable nanocarrier system for targeted anticancer drug delivery. J Control Release. 2010; 144: 314–323
139. Filippousi M, Papadimitriou SA, Bikiaris DN, et al. Novel core-shell magnetic nanoparticles for PTX encapsulation in biodegradable and biocompatible block copolymers: Preparation, characterization and release properties. Int J Pharm. 2013; 448: 221–230
140. Bakewell SJ, Carie A, Costich TL, et al. Imaging the delivery of drug-loaded, iron-stabilized micelles. Nanomedicine. 2017; 13: 1353–1362
141. Schleich N, Sibret P, Danhier P, et al. Dual anticancer drug/superparamagnetic iron oxide-loaded PLGA-based nanoparticles for cancer therapy and magnetic resonance imaging. Int J Pharm. 2013; 447: 94–101
142. Wang J, Gong C, Wang Y, et al. Magnetic nanoparticles with a pH-sheddable layer for antitumor drug delivery. Colloids Surf B. 2014; 118: 218–225
143. Yang X, Grailer JJ, Rowland IJ, et al. Multifunctional SPIO/DOX-loaded wormlike polymer vesicles for cancer therapy and MR imaging. Biomaterials. 2010; 31: 9065–9073
144. Patra HK, Khaliq NU, Romu T, et al. MRI-visual order-disorder micellar nanostructures for smart cancer theranostics. Adv Healthc Mater. 2014; 3: 526–535
145. Wang H, Wang S, Liao Z, et al. Folate-targeting magnetic core-shell nanocarriers for selective drug release and imaging. Int J Pharm. 2012; 430: 342–349
146. Ji W, Li N, Chen D, et al. A hollow porous magnetic nanocarrier for efficient near-infrared light- and pH-controlled drug release. RSC Adv. 2014; 4: 51055–51061
147. Nasongkla N, Bey E, Ren J, et al. Multifunctional polymeric micelles as cancer-targeted, MRI-ultrasensitive drug delivery systems. Nano Lett. 2006; 6: 2427–2430
148. Gao X, Luo Y, Liao C. Prostate stem cell antigen-targeted nanoparticles with dual functional properties : in vivo imaging and cancer chemotherapy. Int J Nanomedicine. 2012; 7: 4037–4051
149. Chertok B, David AE, Huang Y, et al. Glioma selectivity of magnetically targeted nanoparticles: A role of abnormal tumor hydrodynamics. J Control Release. 2007; 122: 315–323
150. Yang HW, Hua MY, Liu HL, et al. Self-protecting core-shell magnetic nanoparticles for targeted, traceable, long half-life delivery of BCNU to gliomas. Biomaterials. 2011; 32: 6523–6532
151. Liao J, Wei X, Ran B, et al. Polymer hybrid magnetic nanocapsules encapsulating IR820 and PTX for external magnetic field-guided tumor targeting and multifunctional theranostics. Nanoscale. 2017; 9: 2479–2491
152. Zhu K, Deng Z, Liu G, et al. Photoregulated cross-linking of superparamagnetic iron oxide nanoparticle (SPION) loaded hybrid nanovectors with synergistic drug release and magnetic resonance (MR) imaging enhancement. Macromolecules. 2017; 50: 1113–1125
153. Asadi H, Khoee S, Deckers R. Polymer-grafted superparamagnetic iron oxide nanoparticles as a potential stable system for magnetic resonance imaging and doxorubicin delivery. RSC Adv. 2016; 6: 83963–83972
154. Biswas D, Li P, Liu D, et al. Enhanced encapsulation of superparamagnetic Fe_3O_4 in acidic core-containing micelles for magnetic resonance imaging. RSC Adv. 2015; 5: 107938–107948
155. Feng ST, Li J, Luo Y, et al. pH-sensitive nanomicelles for controlled and efficient drug delivery to human colorectal carcinoma LoVo cells. PLoS One. 2014; 9: e100732
156. Kuppusamy P, Li H, Ilangovan G, et al. Noninvasive imaging of tumor redox status and its modification by tissue glutathione levels noninvasive imaging of tumor redox status and its modification by tissue. Cancer Res. 2002; 62: 307–312
157. Yu J, Li X, Luo Y, et al. Poly(ethylene glycol) shell-sheddable magnetic nanomicelle as the carrier of doxorubicin with enhanced cellular uptake. Colloids Surf B. 2013; 107: 213–219
158. Ding M, Zeng X, He X, et al. Cell internalizable and intracellularly degradable cationic polyurethane micelles as a potential platform for efficient imaging and drug delivery. Biomacromolecules. 2014; 15: 2896–2906
159. Kievit FM, Gunn JW, Lee D. PEI-PEG-chitosan copolymer coated iron oxide nanoparticles for safe gene delivery: Synthesis, complexation, and transfection. Adv Funct Mater. 2009; 19: 2244–2251
160. Kievit FM, Veiseh O, Fang C, et al. Chlorotoxin labeled magnetic nanovectors for targeted gene delivery to glioma. ACS Nano. 2010; 4: 4587–4594
161. Stephen ZR, Dayringer CJ, Lim JJ, et al. Approach to rapid synthesis and functionalization of iron oxide nanoparticles for high gene transfection. ACS Appl Mater Interfaces. 2016; 8: 6320–6328
162. Wang C, Ravi S, Martinez GV, et al. Dual-purpose magnetic micelles for MRI and gene delivery. J Control Release. 2012; 163: 82–92
163. Lee SJ, Muthiah M, Lee HJ, et al. Synthesis and characterization of magnetic nanoparticle-embedded multi-functional polymeric micelles for MRI-guided gene delivery. Macromol Res. 2012; 20: 188–196
164. Wan Q, Xie L, Gao L, et al. Self-assembled magnetic theranostic nanoparticles for highly sensitive MRI of minicircle DNA delivery. Nanoscale. 2013; 5: 744–752
165. Lee SY, Yang CY, Peng CL, et al. A theranostic micelleplex co-delivering SN-38 and VEGF siRNA for colorectal cancer therapy. Biomaterials. 2016; 86: 92–105
166. Wang C, Hsu CH, Li Z, et al. Effective heating of magnetic nanoparticle aggregates for in vivo nano-theranostic hyperthermia. Int J Nanomedicine. 2017; 12: 6273–6287
167. Xie J, Zhang Y, Yan C, et al. High-performance PEGylated Mn-Zn ferrite nanocrystals as a passive-targeted agent for magnetically induced cancer theranostics. Biomaterials. 2014; 35: 9126–9136
168. Huang X, El-Sayed IH, Qian W, et al. Cancer cell imaging and photothermal therapy in the near-infrared region by using gold nanorods. J Am Chem Soc. 2006; 128: 2115–2120
169. Li J, Hu Y, Yang J, et al. Hyaluronic acid-modified Fe_3O_4 at Au core/shell nanostars for multimodal imaging and photothermal therapy of tumors. Biomaterials. 2015; 38: 10–21
170. Dong W, Li Y, Niu D, et al. Facile Synthesis of monodisperse superparamagnetic Fe_3O_4 core@hybrid@Au shell nanocomposite for bimodal imaging and photothermal therapy. Adv Mater. 2011; 23: 5392–5397
171. Chen H, Ren X, Paholak HJ, et al. Facile fabrication of near-infrared-resonant and magnetic resonance imaging-capable nanomediators for photothermal therapy. ACS Appl Mater Interfaces. 2015; 7: 12814–12823
172. Yang J, Lee CH, Ko HJ, et al. Multifunctional magneto-polymeric nanohybrids for targeted detection and synergistic therapeutic effects on breast cancer. Angew Chem Int Ed Engl. 2007; 46: 8836–8839
173. Liu Y, Yang K, Cheng L, et al. PEGylated FePt@Fe2O3core-shell magnetic nanoparticles: Potential theranostic applications and in vivo toxicity studies. Nanomedicine. 2013; 9: 1077–1088
174. Tang H, Guo Y, Peng L, et al. In vivo targeted, responsive, and synergistic cancer nanotheranostics by magnetic resonance imaging-guided synergistic high-intensity focused ultrasound ablation and chemotherapy. ACS Appl Mater Interfaces. 2018; 10: 15428–15441
175. Purushotham S, Chang PEJ, Rumpel H, et al. Thermoresponsive core-shell magnetic nanoparticles for combined modalities of cancer therapy. Nanotechnology. 2009; 20: 305101
176. Zhen Z, Xie J. Development of manganese-based nanoparticles as contrast probes for magnetic resonance imaging. Theranostics. 2012; 2: 45–54
177. Tong G, Fang Z, Huang G, et al. Gadolinium/DOTA functionalized poly(ethylene glycol)-block-poly(acrylamide-co-acrylonitrile) micelles with synergistically enhanced cellular uptake for cancer theranostics. RSC Adv. 2016; 6: 50534–50542
178. Huang S, Cheng Z, Chen Y, et al. Multifunctional polyelectrolyte multilayers coated onto Gd_2O_3 : Yb^{3+}, Er^{3+}@ MSNs can be used as drug carriers and imaging agents. RSC Adv. 2015; 5: 41985–41993
179. Tian S, Liu G, Wang X, et al. pH-responsive tumor-targetable theranostic nanovectors based on core crosslinked (CCL) micelles with fluorescence and magnetic resonance (MR) dual imaging modalities and drug delivery performance. Polym (Basel). 2016; 8: 1–18
180. Ho LC, Hsu CH, Ou CM, et al. Unibody core-shell smart polymer as a theranostic nanoparticle for drug delivery and MR imaging. Biomaterials. 2015; 37: 436–446
181. Yao J, Hsu C-H, Li Z, et al. Magnetic resonance nano-theranostics for glioblastoma multiforme. Curr Pharm Des. 2015; 21: 5256–5266
182. Caltagirone C, Falchi AM, Lampis S, et al. Cancer-cell-targeted theranostic cubosomes. Langmuir. 2014; 30: 6228–6236
183. Zhang L, Yang Z, Zhu W, et al. Dual-stimuli-responsive, polymer-microsphere-encapsulated cus nanoparticles for magnetic resonance imaging guided synergistic chemo-photothermal therapy. ACS Biomater Sci Eng. 2017; 3: 1690–1701
184. Li M, Li L, Zhan C, et al. Core-shell nanostars for multimodal therapy and imaging. Theranostics. 2016; 6: 2306–2313
185. Hu DR, Chen LJ, Qu Y, et al. Oxygen-generating hybrid polymeric nanoparticles with encapsulated doxorubicin and chlorin e6 for trimodal imaging-guided combined chemo-photodynamic therapy. Theranostics. 2018; 8: 1558–1574
186. Wang L, Li D, Hao Y, et al. Gold nanorod – based poly (lactic-co-glycolic acid) with manganese dioxide core – shell structured multifunctional nanoplatform for cancer theranostic applications. Int J Nanomedicine. 2017; 12: 3059–3075
187. Liu J, Chen Q, Zhu W, et al. Nanoscale-coordination-polymer-shelled manganese dioxide composite nanoparticles: A multistage redox/pH/H_2O_2-responsive cancer theranostic nanoplatform. Adv Funct Mater. 2017; 27: 1605926
188. Chen Q, Wang X, Wang C, et al. Drug-induced self-assembly of modified albumins as nano-theranostics for tumor-targeted combination therapy. ACS Nano. 2015; 9: 5223–5233
189. Sun X, Zhang M, Du R, et al. A polyethyleneimine-driven self-assembled nanoplatform for fluorescence and MR dual-mode imaging guided cancer chemotherapy. Chem Eng J. 2018; 350: 69–78

190. Deng X, Dai Y, Liu J, et al. Multifunctional hollow CaF_2: $Yb^{3+}/Er^{3+}/Mn^{2+}$-poly(2-Aminoethyl methacrylate) microspheres for Pt(IV) pro-drug delivery and tri-modal imaging. Biomaterials. 2015; 50: 154–163
191. Porsch C, Zhang Y, Östlund Å, et al. In vitro evaluation of non-protein adsorbing breast cancer theranostics based on 19F-polymer containing nanoparticles. Part Part Syst Charact. 2013; 30: 381–390
192. Boissenot T, Fattal E, Bordat A, et al. Paclitaxel-loaded PEGylated nanocapsules of perfluorooctyl bromide as theranostic agents. Eur J Pharm Biopharm. 2016; 108: 136–144
193. Quang HV, Chang C, Song P, et al. Caveolae-mediated mesenchymal stem cell labelling by PSS-coated PLGA PFOB nano-contrast agent for MRI. Theranostics. 2018; 8: 2657–2671
194. Wijagkanalan W, Kawakami S, Hashida M. Designing dendrimers for drug delivery and imaging: Pharmacokinetic considerations. Pharm Res. 2011; 28: 1500–1519
195. Boyd BJ, Kaminskas LM, Karellas P, et al. Cationic poly-l-lysine dendrimers: pharmacokinetics, biodistribution, and evidence for metabolism and bioresorption after intravenous administration to rats. Mol Pharm. 2006; 3: 614 –627
196. Leiro V, Garcia JP, Tomás H, et al. The present and the future of degradable dendrimers and derivatives in theranostics. Bioconjug Chem. 2015; 26: 1185–1197
197. Lee SJ, Jeong JR, Shin SC, et al. Nanoparticles of magnetic ferric oxides encapsulated with poly(D,L latide-co-glycolide) and their applications to magnetic resonance imaging contrast agent. J Magn Magn Mater. 2004; 272: 2432–2433
198. Kwon HY, Lee JY, Choi SW, et al. Preparation of PLGA nanoparticles containing estrogen by emulsification-diffusion method. Colloids Surf A. 2001; 182: 123–130
199. Lemoine D, Francois C, Kedzierewicz F, et al. Stability study of nanoparticles of poly(e-caprolactone), poly(D,L-lactide) and poly(D,L-lactide-co-glycolide). Biomaterials. 1996; 17: 2191–2197
200. Danhier F. To exploit the tumor microenvironment: since the EPR effect fails in the clinic, what is the future of nanomedicine?. J Control Release. 2016; 244: 108-121.